A ROBOT TO MEASURE WATER PARAMETERS IN WATER DISTRIBUTION SYSTEMS

A Dissertation

by

SABER KAZEMINASAB HASHEMABAD

Submitted to the Graduate and Professional School of
Texas A&M University
in partial fulfillment of the requirements for the degree of

DOCTOR OF PHILOSOPHY

Chair of Committee,	Roozbeh Jafari
Committee Members,	M. Katherine Banks
	Hangue Park
	Pao-Tai Lin
Head of Department,	Miroslav M. Begovic

December 2021

Major Subject: Computer Engineering

ABSTRACT

Water distribution systems (WDS) are critical infrastructures that transfer drinking water to consumers. In the U.S., around 42 billion gallons of water are being delivered per day via one million miles of pipes to be used in different sectors. Incidents to pipelines cause leak or let contaminants enter purified water in pipe that is harmful to public health. Hence, periodic condition assessments of pipelines and water inside it are required. However, due to the long and complicated configurations of these networks, access to all parts of the pipelines is a cumbersome task. To this aim, in-pipe robots are promising solution that facilitate access to different locations inside pipelines and perform different in-pipe missions.

In this project, we design and fabricate an in-pipe robotic system is that is used for water quality monitoring. The robot is equipped with a wireless sensor module and the sensor module is synchronized with the motion unit of the robot. The wireless sensor module facilitates bi-directional data transmission between the robot and base station aboveground. The integrated robotic system navigates in different configurations of the pipeline with smart motion.

To this aim, the mechanical design of the self-powered robot based on three adjustable arm modules and three actuator modules is designed. The components of the robot are characterized based on real operation conditions in pipes. A multi-phase motion control algorithm is developed for the robot to move in straight path and non-straight configurations like bends and T-junctions. A bi-directional wireless sensor module is designed to send data packets through underground environment. Finally, the multi-phase motion controller is synchronized with the wireless sensor module and we propose an operation procedure for the robot. In the operation procedure, some radio transceivers are located at non-straight configurations of pipelines and receive the sensor measurements from the robot and guide the robot in the desired direction. The proposed operation procedure provides smart navigation and data transmission during operation for the robot.

DEDICATION

To my wife, my mother, and my father.

ACKNOWLEDGEMENTS

Professors M. Katherine Banks and Roozbeh Jafari, my advisers, have taught, guided, supported, and encouraged me over the last three years. They helped me to become an independent researcher who thinks critically and follows the facts. I would like to express my deepest gratitude and respect to my advisers among all I have worked with so far. I would like to extend my sincere appreciation to my committee members: Dr. H. Park, and Dr. P. Lin. They provided me with encouragement and patience throughout the prelim and final exams. Dr. H. Park gave me interesting and meaningful questions to my dissertation and Dr. P. Lin helped me to have practical perspectives of my dissertation. I would also extend my gratitude to Dr. S. Biswas, Dr. S. Rajagopalan, and Dr. M. Lagoudas from the Division of Commercialization & Entrepreneurship in Texas A&M Engineering Experiment Station (TEES). They encouraged me and expressed their sympathy by sharing their valuable thoughts and advice to have a system for real applications. I also appreciate Dr. S. M. Wright for his time and valuable comment on one of the most challenging parts of my project. I had the great pleasure of working with the Embedded Signal Processing (ESP) team: Ali Akbari, Kaan Sell, Bassem Ibrahim, Muhammad Emaduddin, Jonathan Martinez, I would like to express warm gratitude to my family. My wife, mom, and dad supported me in all directions. This dissertation is dedicated to them and their unconditional support. I have met precious colleagues: Dr. D. Kalathil, Dr. A. Wang, Dr. Anxiao (Andrew) Jiang, Dr. Guni Sharon, Dr. S. L. Miller. Their passion for research and work enlightened and stimulated me. Special thanks to cool and awesome friends: Mohsen Aghashahi, Rouxi Wu, Moein Razavi, Hamed Alikhani, Mohammad Aghajani, Hamed Farahmand, Reza Ghiri, Hananeh Alambeigi, Dr. Maryam Zahabi, Ehsan Hajramezanali, Mostafa Karimi, Arman Hasanzadeh, Peiman Mohseni, Samira Ziadidegan, Roya Pashmfroosh, Aria Hasanzadeh Zonuzy, Negar Beyki, Dr. Hamidreza Samoei, Mahmood Tabesh, Shahriar Esmaeili , Moein Nazifi, Nandita Chturvedi.

CONTRIBUTORS AND FUNDING SOURCES

Contributors

This work was supervised by a dissertation committee consisting of Professor M. Katherine Banks, of the Zachry Department of Civil and Environmental Engineering, Professor Roozbeh Jafari, Dr. Haunge Park, and Dr. Pao-Ti Lin of the Department of Electrical and Computer Engineering.

All work for the dissertation was completed by the student, under the advisement of Professor M. Katherine Banks of the Zachry Department of Civil and Environmental Engineering and Professor Roozbeh Jafari of the Department of Electrical and Computer Engineering.

Funding Sources

There are no outside funding contributions to acknowledge related to the research and compilation of this document.

TABLE OF CONTENTS

Page

LIST OF FIGURES

Page

LIST OF TABLES

Page

1. INTRODUCTION

1.1. Significance of the In-pipe Robots

Water distribution systems (WDS) [1] are critical infrastructures that transfer drinking water to consumers (Figure 1.1). In the U.S. about 42 billion gallons of water per day are being delivered via one million miles of pipes to be used in daily life, factories, and offices across the country. The U.S. Environmental Protection Agency (EPA) has set regulations that enforce drinking water utilities to limit the levels of contaminants in drinking water [2]. These contaminants can be introduced to water pipes by accidental or deliberate incidents.

Moreover, aging water infrastructures [3]–[5] have experienced an increase in break rate. One of the significant consequences of pipe breaks is negative pressure at cross-connections where surrounding non-potable substances come to contact with the potable water in a pipeline and cause public health crises. EPA reported 9,734 water-borne diseases due to cross-connections between 1981 to 1998 [2]. Hence, it requires water utilities to monitor their potable water supplies by regular water sampling and laboratory analyses to ensure the drinking water standards are met.

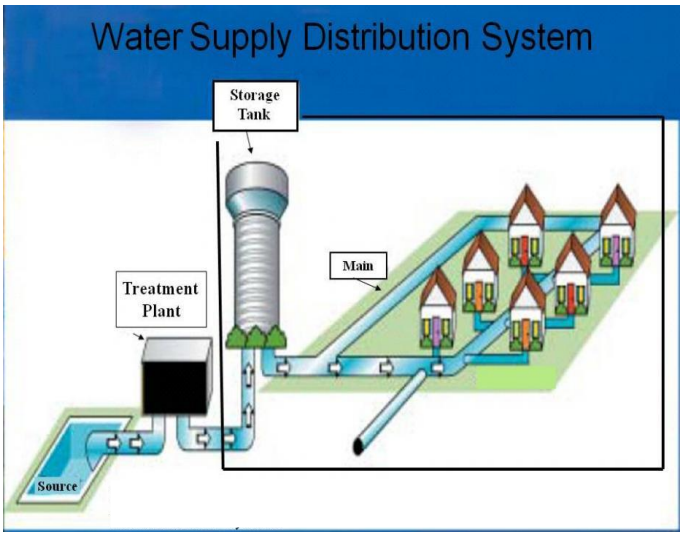

Figure 1.1. The Schematic of Water Distribution System.
Source: Adapted from [1].

These laboratory-based methods, however, are too slow and are not efficient for contamination detection [6]. Although stationary water quality sensors (placed outside of a pipe with their probes measuring flowing water quality) are recommended tools for online monitoring, due to their expensive deployment and maintenance, establishing a ubiquitous network of these sensors is burdensome [7]. The cost challenges have set a constraint on the number of stationary sensors that can be placed at a network. This problem prevents a water utility from having a stationary sensing network with good spatiotemporal coverage along pipelines. Inline free-swimming sensors that move in a pipe with flowing water have emerged as stand-alone or complementary solutions for real-time water quality monitoring [8], or leak detection in water pipelines [9], [10]. These mobile sensors can be useful when a water quality abnormality or leak is reported in pipe segments that are not monitored by stationary sensors. In this case, an operator can insert a free-swimming sensor from a fire hydrant into a suspicious water pipeline, and it rolls through the desired location for more accurate measurement and monitoring. However, the implementation difficulties of these mobile sensors are twofold: i) the sensors disrupt the normal operation of a water network [11], and ii) each sensor may take random path at junctions based on flow conditions [10], [12]. To implement free-swimming sensors, a water utility should stop the operation of its network and manipulate valves and pumps to deliver the sensor to the desired location. This problem adversely affects network performance and also makes water utilities reluctant to use the sensors. Moreover, due to the absence of enough control over the sensor motion in a pipe, their temporal or permanent loss has been reported by utilities. Inline robots have been developed and deployed for pipe inspection. However, there are some challenges for inline robots such as vertical mobility, size adaptability, stability, driving capacity, and wireless control capability. The existing inline robots are not well-equipped for application in real-time water quality monitoring in WDSs. Therefore,

there is a need for an automated robot that is customized for miniaturized water quality sensors and is capable of operation in a potable water distribution system without disturbing the network services.

1.2. Previous Work

There are different aspects of in-pipe robotic systems that need to be considered. Since the operating environment of these robots is a confined space of pipelines, the factors like mechanism, motion control strategy, power source, and wireless communication are closely associated together. Mechanisms in robots are referred to power transmission mechanism that delivers the actuator's power to the moving part(s) of the robot. For in-pipe robots, the mechanisms are divided into three parts and eight subparts [13]; The main mechanisms are wheeled robots, caterpillar robots, and without wheels robots. As its name defines, in the wheeled robots, the wheels move the robot inside pipe. In the caterpillar robots, the belts are connected to the wheels. The robots without wheels move inside the pipe with components other than wheels. The wheeled robots are divided into simple structures, wall-pressed, and screw-drive types. In simple structures, wheels are directly connected to the body of the robot and makes control over the speed of the robot easy and accurate [14], [15]. In the wall-pressed robots however, the wheels press the pipe wall with adjustable arms that are usually anchored to the body of the robot with 120° angle [9], [16]–[18]. Screw-type robots are another type in which use a pair of rotational and stationary modules to covert the radial spiral motion of the rotational module to the linear motion of the robot along the axis of the pipe [19]. In the without-wheel-robots, other mechanisms like "legs" [20] or bio-inspired motions (like inchworm locomotion [21]–[23] and snake motion [24]) are used. The without-wheel robots can pass through different configurations of the pipelines like bends and T-junctions. However, their velocity is slow and requires a rather complex motion control algorithm [13]. Pipelines have different sizes and the robot may encounter different sizes during operation.

Hence, the robot should be able to adapt to different pipe diameters. Some robots adapt to a specific pipe size [25], [26] while others are adaptable to the internal size of pipes [16], [21], [27]–[43].

Different actuators drive in-pipe robots to provide power for motion. Pneumatic actuators [21], [25] and electrical actuators (i.e. DC motors) [16], [27], [33], [37], [43] are common types that are used in in-pipe robots. Since the pneumatic-operated robots use special power transmission mechanisms, they are less common in in-pipe robots due to space limitation. Also, a new type of actuators based on shape memory alloys (SMA) are used for motion power. However, due to their highly nonlinear electro-thermomechanical behavior, complex controllers are needed to control their motion [44] that make them infeasible to implement. Power supply in in-pipe robots is crucial to their applicability as distribution networks comprise long lines of pipes and the in-pipe robots need to inspect long-distance of the pipeline. Some robots are powered with cable [18], [30], [38]–[41] in which the short length of cables limits their inspection length. Few robots are battery-powered [16]. Since the environment of pipelines are highly pressurized and a high-speed flow is present [45], operation conditions need to be considered among battery-powered robots and this problem is not well addressed [46].

Pipelines in WDS comprise complicated configurations in which the in-pipe robot need to pass through [13]. The researchers try to develop motion control algorithms for straight paths [47], [48], and non-straight paths like bends and T-junctions [37], [49]–[51]. However, the challenge of smart navigation (in which the robot selects the appropriate motion control algorithm during operation) is open for further studies. Data transmission in in-pipe robots is another aspect that needs to be considered. It is possible to exchange data between robot and base station (BS) through wired communication among tethered robots. However, due to limited inspection length, cable-operated robots are not desired based on the feedback from water utility managers. Wireless communication

is a promising solution for data transmission in these robots in which the robot moves inside the pipeline and the wireless sensor module is mounted on it and the receiver(s) is located outside the pipeline (either on pipe or aboveground) and the data is transmitted between them. However, wireless communication is challenging in the environment of soil, rock, and water, due to high signal attenuation [52], and also, the communication channel is highly dynamic as the variable water content of soil affects the path loss as well as the sand-clay composition of soil [52]. Based on Friis propagation theory [53], using a low-frequency carrier signal results in better penetration in the harsh environment that helps to mitigate signal attenuation at the expense of larger antenna sizes. Magnetic Induction (MI) communication is a solution that mitigates the challenges mentioned for EM waves. In this method, a pair of coils act as antennas that transmits and receives data based on mutual induction [54]. Sun et al. modeled the MI communication channel and provided a relation for the received signal's power to the transmitted signal's power. To increase the read range of the MI communication link, they utilized waveguide coils that are parallel to the pipe axis and are mounted on the pipe's circumference [54]. Tan et al. verified the feasibility of waveguides with experimental results in [55]. Communication efficiency in MI communication method depends on the direction of the transmitter and receiver coils dramatically in which the coils need to be parallel and if there is a misalignment angle between their normal axes, the efficiency of the communication link drops, drastically [55]. To address this challenge, omni-directional coil antennas are proposed in [56]. However, the size of these antennas limits their applicability for confined spaces in the pipe environment. Although the MI communication remains efficient in stationary sensor networks and mobile sensor networks, its use is a challenging task and needs complicated mechanisms for a reliable communication link. For the in-pipe robots however, EM-based wireless modules show better performance due to the miniaturization of

commercial wireless transceivers. Researchers employ EM waves with supplementary mechanisms to facilitate reliable communication [57].

1.3. Technical Gaps in In-pipe Robots

Based on the study of the current works, the technical gaps in the field of in-pipe robots can be summarized as:

- A reliable wireless communication link is needed in the harsh environment of the propagation medium.
- To the best of our knowledge, there is not a reliable robotic system that can be used for water quality monitoring in distribution systems with large pipe diameters.
- In WDSs, the range of pipe size variation is high compared to other types of networks. There is no robotic system that can adapt to this range of diameter change.
- The operating environment in these applications is high-pressure pipelines in which a flow is present. Hence, it requires a robust and reliable motion during operation.
- The mobility, control, wireless communication modules of mobile sensor modules need to be synchronized to achieve smart navigation during the inspection. Smart navigation makes the robot negotiate special configurations, inclinations, and uncertainties in the network.
- A long and complicated pipeline network requires inspection methods to cover sufficiently large distances of pipelines. Hence, the power supply is of paramount importance in inspection purposes and the tethered robots are no longer feasible to use.
- Pipelines comprise different configurations like straight paths, bends, Wyes, Tees. The in-pipe robots need a mechanism and motion control algorithm that facilitate motion in these configurations.

1.4. Our Objective

The main objective of our research is to design an in-pipe robotic system that is used for long pipe inspection with the aim of both water quality monitoring and leak detection in water distribution systems (WDS) while the system remains in service. We plan to address the following gaps in in-pipe robots in this project:

- The maneuverability of In-pipe Robots in Complicated Configurations of Distribution Systems.

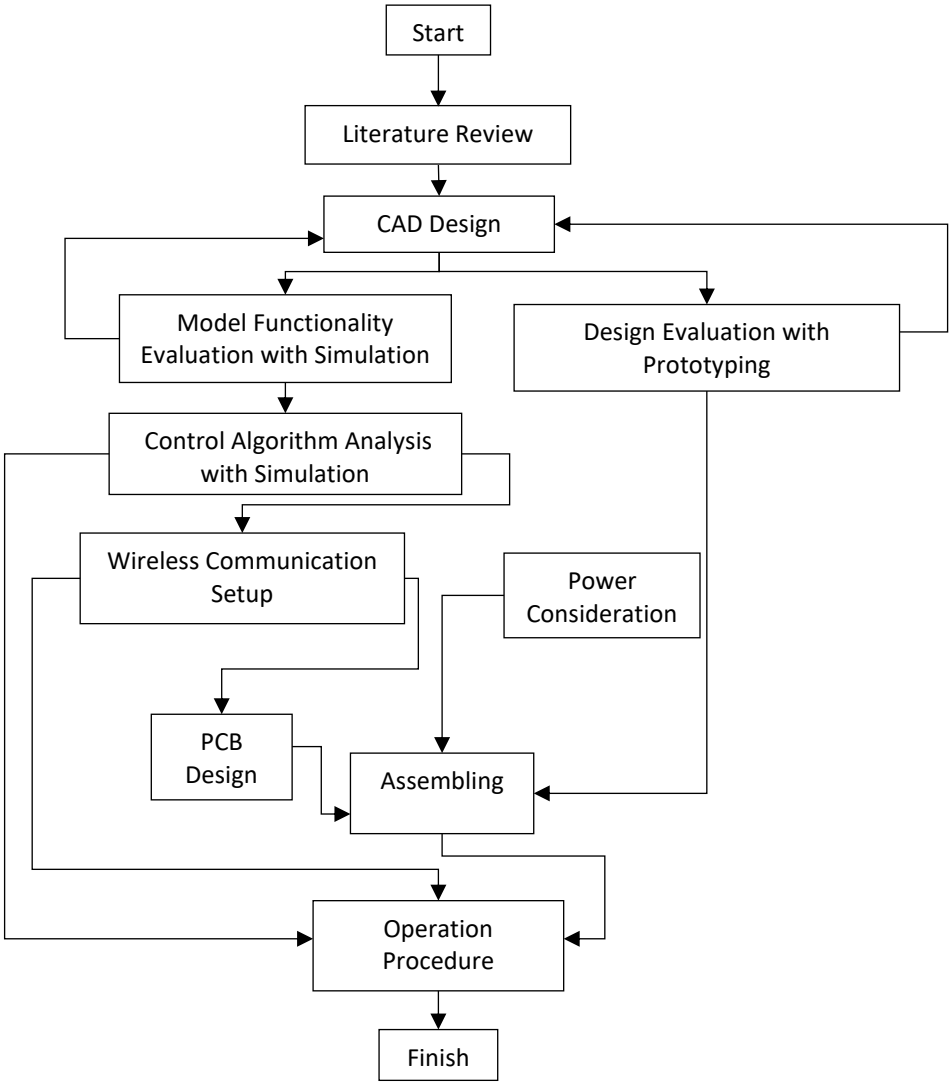

Figure 1.2. Proposed Methodology for System Design and Implementation in this Project.

- Agility of in-pipe robots in in-service distribution networks is not well-addressed in the literature.
- Wireless underground data transmission during operation is a challenge for in-pipe robots.
- Long-distance inspection with smart navigation for in-pipe robots is the most challenging task and is open for further research.

1.5. Our Approach

Our approach is based on an under-actuated wall-press wheeled robot that is self-powered and moves inside different configurations of pipelines with a multi-phase motion control algorithm and a bi-directional wireless sensor module. The sensor module is located inside the robot and measures the target parameters in water (e.g. PH, conductivity, turbidity, etc.). We then synchronize the wireless sensor module with the multi-phase motion control algorithm and develop an algorithm for smart navigation of the robot in distribution systems.

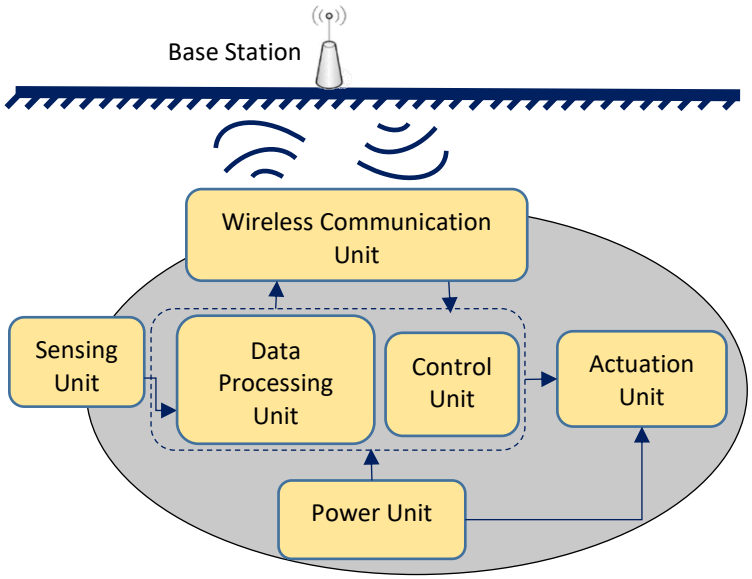

Figure 1.3. The Schematic of Our Proposed Robotic System.

The components of the robot affect the functionality of each other; hence, we proposed a methodology that defines the procedure of the system design and implementation (Figure 1.2). In figure 1.3, the overall view of the components of the proposed system and their interactions are shown. The sensing unit measures the concentration of the target analytes. The sensor measurements are then processed by a data processing unit to have the correct value for the associated parameter. The task of the control unit is to control the motion of the robot during operation. The actuation unit moves the robot inside the robot and the power unit provides electrical power for robot's components during operation.

1.6. Notes and References

Current systems for water quality monitoring and leak detection are not efficient as they are slow (i.e. laboratory-based method [6]), limited to a small area (i.e. stationary sensor networks [7]), and disrupt the normal operation of the distribution system (i.e. mobile sensors [58]). To address these challenges, we design an in-pipe robot (with independent motion of flow motion in in-service networks) that can be used for both water quality monitoring [58] and leak detection [59] in water distribution systems. The robot integrates a size-adaptable, wheeled, wall-press, and self-powered mechanical system, a sensing unit for quality monitoring [60] and leak detection [61], a multi-phase motion control algorithm [49], and a wireless sensor module that addresses the challenges of wireless underground communication presented in [52]. We also propose an operation procedure for the robot by integrating the robot, the multi-phase motion control algorithm, and the wireless system to address the challenges of localization [57], [62]–[66], navigation [67]–[70], and long-distance inspection [71] of in-pipe robots in in-service distribution systems.

2. DESIGN AND PROTOTYPING OF THE IN-PIPE ROBOT*

2.1. Introduction

The mechanism of the robot affects other parameters of the system since all components are mounted on the robot and the operating environment of the robot is pipes in which pressurized water flow is present (and impose space limitation on the robot). The line pressure of the flow ranges between 100 kPa and 500 kPa [9] and its velocity ranges from 0.5 m/s to 2.5 m/s [45] in which applies a lot of mechanical stress on the robot's components during operation. Since the operation environment of the robot is pipes where potable water is present, one important factor in the design of robot is health issues. The robot comprises electronic and mechanical parts that may contain materials that are toxic to human health. The design of the robot needs to be in a way that does not release these materials to water and also prevents water to damage the electronic elements of the robot.

In this chapter, we design the mechanical system of a modular size-adaptable in-pipe robot that embeds the electronics components, sensor module, and power supply. The robot moves in the pipe by pressing the pipe wall that is facilitated by three adjustable arm modules and three actuator modules and are anchored on a central processor. The actuator modules convert the rotational motion of the wheels to linear motion for the robot along the pipe axis.

To design a fully automotive system, we characterized the robot's components based on operation conditions.

*Part of this chapter is reprinted with permission from "Design, Characterization, and Control of a Size Adaptable In-pipe Robot for Water Distribution Systems" by Saber Kazeminasab, Ali Akbari, Roozbeh Jafari, M. Katherine Banks. 2021. IEEE International Conference on Industrial Technology (ICIT), Vol. 1, pp. 39-46, Copyright 2021 by IEEE.

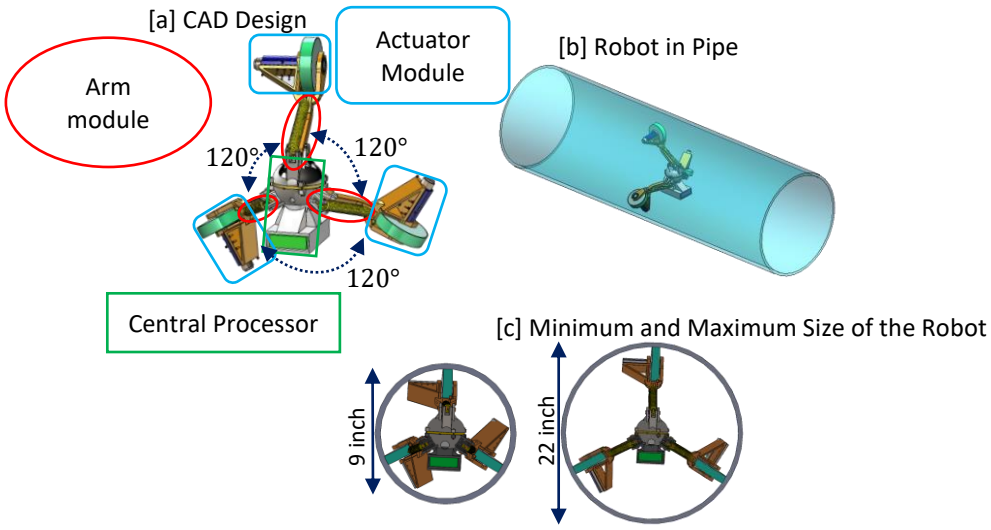

Figure 2.1. Robot Design.

2.2. Design of the In-pipe Robot

The mechanical design of the robot is based on a size-adaptable wheeled wall-press mechanism. Figure 2.1 shows the overall view of the robot and its modules in which are:

- One Central Processor.
- Three Arm Modules.
- Three Actuator Modules.

Our robot design is modular which makes assembling, disassembling, and maintenance of the robot easy. In the following, we will explain each module in detail.

2.2.1. Central Processor

The central processor is composed of two hemisphere-like parts (see figure 2.2). One hemisphere ([a] in figure 2.2a) includes a sensing module that includes miniaturized chemical sensors and a micro-pump system. The micro-pump provides water samples by circulating water from the water inlet and outlet holes indicated as ([j] in figure 2.2a). This hemisphere is called the sensing part for brevity. The other hemisphere ([d] in figure 2.2a), the so-called control part,

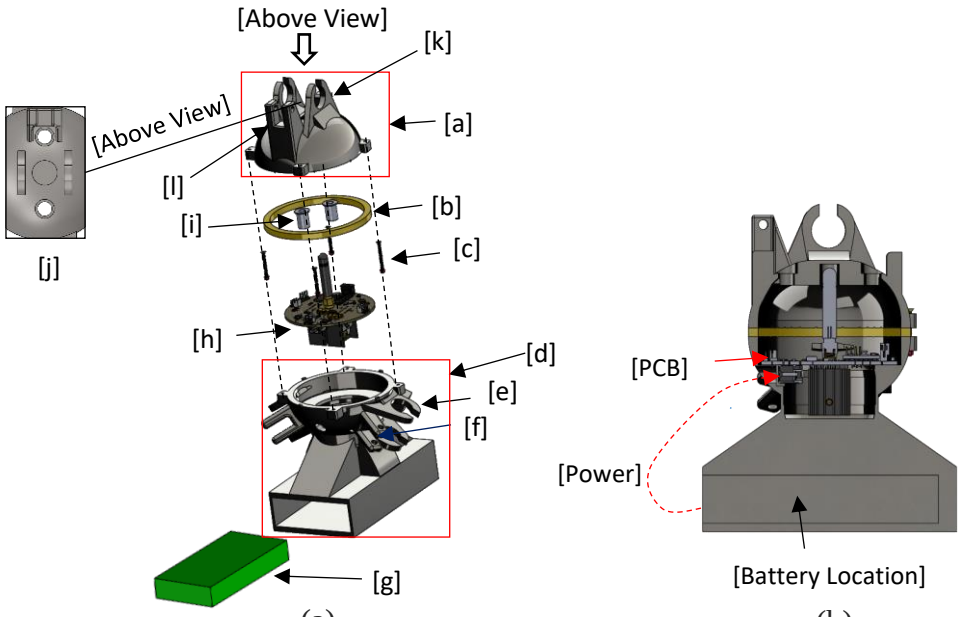

(a) (b)

Figure 2.2. Central Processor (a) Exploded View. (b) Cross Section View.

controls the timing of the operation of the sensors, actuators, the motion control unit, and the wireless sensor module. The electronic components are embedded in the printed circuit board (PCB) ([h] in figure 2.2a). We will describe the design of the PCB later. To protect the PCB inside the central processor, a seal mechanism was designed where a standard off-the-shelf O-ring locates between the hemispheres ([b] in figure 2.2a). Then the hemispheres are fastened with four pairs of screws and nuts which push the O-ring ([c] in figure 2.2a). This sealing design keeps the sphere waterproofed and away from wear and tear. Per arm, there is a base to attach it to the sphere with ball bearings ([k] and [e] in figure 2.2a). Spring anchors connect one end of a spring to the sphere ([f] and [l] in figure 2.2a) via metal pins. Power of the battery is transmitted to the control part with wire through a hole as shown in figure 2.2b.

2.2.2. Arm Module

Since water networks comprise pipes with different sizes and configurations, an inline robot should be able to adjust its size based on pipe configuration. The designed robot has three arms in

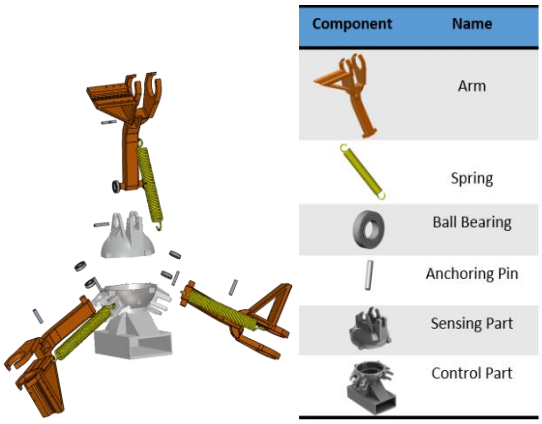

Figure 2.3. Arm Module and the Components.

which have a Boomerang-shape so that they do not obstacle the motion of their springs. To maintain the robot balanced, a passive spring was used for each arm. One end of each spring was attached to the sphere via the anchors (([f] and [l] in figure 2.2a), and another end was connected to the end of the arm (see figure 2.3).

2.2.3. Actuator Module

The actuator module includes a motor cover, a gear-motor, a motor base, screws and nuts to attach the motor and the motor cover to the motor base, a wheel, two ball bearings at both sides of the wheel, and a wheel cover made of rubber (see figure 2.4). The gear motor is at the end of the arms and fixed on the motor basement. To better fix the motors on the bases, the inside surfaces of the motor covers and motor bases were slotted (Figure 2.4). Then these slots were filled with moldable glue. Not only the moldable glue prevents water from penetrating a motor, but it also increases the friction between the motor cover and motor body.

2.3. Robot Characterization

There is a notion of a resilient machine that is first coined in [72] and formulates the requirements for manufacturing a system that is reliable and robust against uncertainties and disturbances during operation. We consider and take the requirements in our work towards a

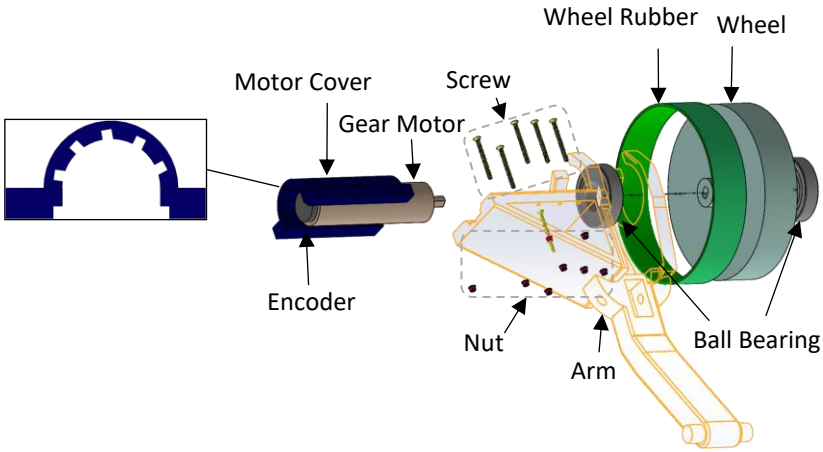

Figure 2.4. CAD Design of the Actuator Module and Its Components.

resilient robot. The robot is supposed to operate in in-service pipelines that are a pressurized environment and a high-velocity potable water flow is present. If the robot get stuck during operation, the network should be shut down, an access point needs to be created on the location of the stuck robot and the robot is retrieved. This is a costly and cumbersome task and hence, the robot needs to be fully automotive during operation. Also, the robot needs to be not a source of toxic materials. We first address the health considerations and then characterize the components of the robot to have fully automotive motion.

2.3.1. Health Considerations in Design

The following considerations were taken to prevent the robot from releasing contaminants:

- The ball bearings are sealed.
- The battery and the actuator module are sealed with moldable glue that isolates them electrically. Also, the battery is waterproof by manufacturer design.
- The moldable glue becomes solid after 24 hours and according to information provided by the glue manufacturer, it does not include toxic materials.
- Since the sensing and control module is sealed, the electronic components inside the sphere are isolated from the outside environment.

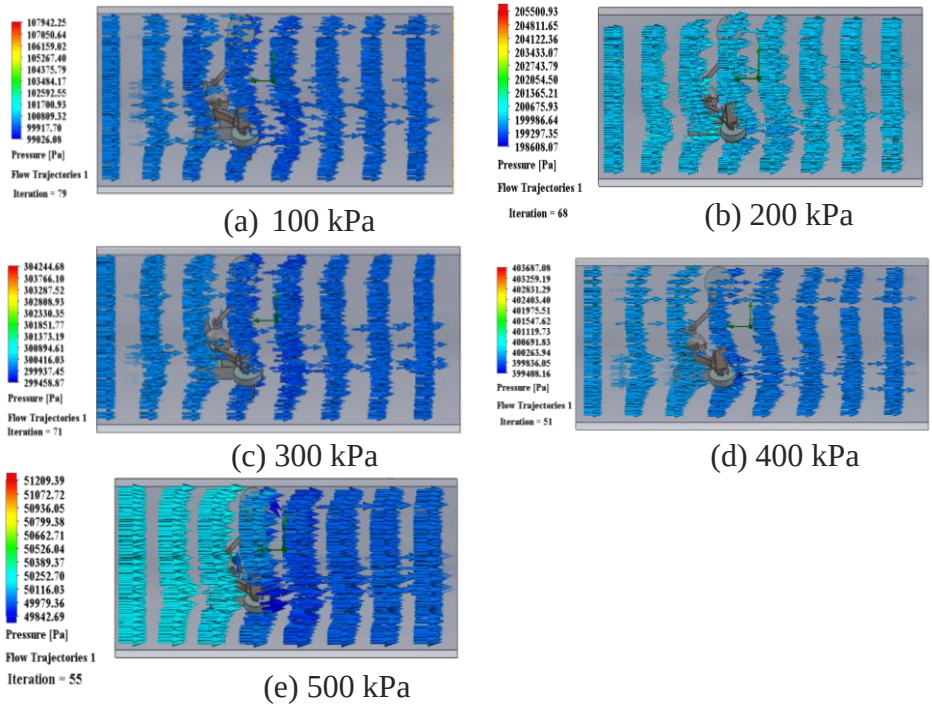

(a) 100 kPa (b) 200 kPa

(c) 300 kPa (d) 400 kPa

(e) 500 kPa

Figure 2.5. Flow Simulations for Line Pressure Effect Evaluation.

2.3.2. Effect of Line Pressure and Relative Velocity on the Robot Performance

Since the robot operates in in-service networks, drag force is applied to the robot because of the relative velocity between the robot and the water flow [73]. Two parameters change the value of drag force during operation: line pressure and relative velocity and in this section, we investigate the effect of each parameter in their range based on standards in distribution systems [74]. To this aim, we simulate the robot in the pipe with flow round in with computational fluid dynamics (CFD) work in SolidWorks software. Our goals in the flow simulations are to find the drag force and also the interference of the robot with the flow during operation.

2.3.2.1. Line Pressure

In this section, we analyze the effect of line pressure on drag force. To this aim, we performed several flow simulations in different line pressures from 100kPa to 500kPa in which

the robot is located in a ≈20-in diameter pipe and a flow with 0.7 m/s velocity in the opposite direction of the robot with 0.5 m/s velocity. The simulations are shown in Figure. 2.5. The colored arrows show the pressure counter around the robot inside pipe. The drag force for each simulation is shown in Table. 2.1. The negative sign of drag force denotes the opposite direction of drag force and the robot motion direction. The results show that there is negligible pressure gradient on both sides of the robot in the pipe. Hence, we can conclude that the robot is minimally invasive to the water flow during operation and this feature of the robot is desirable during operation. Also, an increase in line pressure decreases the drag force applied to the robot. However, this effect is small in which an increase of 400% in line pressure results in a 27% decrease in drag force. Hence, there is no meaningful correlation between the line pressure and the drag force.

Table 2.1. Specification of CFD Simulation and Drag Force Applied on the Robot in Different Line Pressures.

Specification [unit]	**Value**
Fluid Type	Water
Fluid Density [kg/m^3]	1000
Fluid Velocity [m/s]	0.7
Robot Velocity [m/s]	0.5
Pipe Diameter [in]	20
The Relative Direction of Robot and Flow	Opposite
Line Pressure [kPa]	**Drag Force [N]**
100	-25.9
200	-24.4
300	-18.3
400	-19.3
500	-18.9

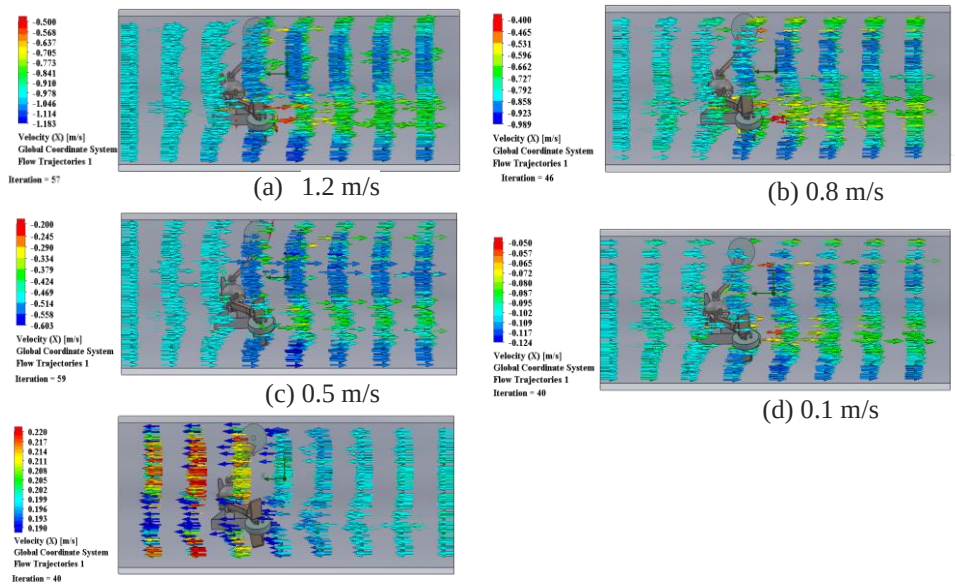

(a) 1.2 m/s (b) 0.8 m/s

(c) 0.5 m/s (d) 0.1 m/s

(e) -0.2 m/s

Figure 2.6. Flow Simulations for Relative Velocity Effect Evaluation.

2.3.2.2. Relative Velocity

In this part, we evaluate the effect of relative velocity on the drag force. To this aim, we did five iterations of flow simulations with 100 kPa line pressure, ≈20-in diameter pipe, and varied velocities. Figure. 2.6 shows the simulations and the velocity counter around the robot in the pipe. In iterations that are shown in figure 2.5a-d, the direction of the robot and flow motions are opposite and in iteration figure 2.5e, their motion is in the same direction. The velocity counters show that the maximum difference in velocity occurs around the wheels and its amount is around 0.2 m/s difference in velocity on both sides of the wheels. The other parts are less invasive to the velocity of the flow. So, in terms of velocity, the robot is minimally invasive to the flow that is desirable in terms of power consumption in the robot. The drag force in each iteration of the simulation is listed in Table. 2.2. The results show that a 700% increase in the relative velocity, results in a 5400% increase in drag force applied on the robot that is a huge amount. Based on the

Table 2.2. Specification of CFD Simulation and Drag Force Applied on the Robot in Different Relative Velocities.

Specification [unit]	**Value**
Fluid Type	Water
Fluid Density [kg/m^3]	1000
Line Pressure [kPa]	100
Pipe Diameter [in]	20
Relative Velocity [m/s]	**Drag Force [N]**
1.2	-25.9
1	-14.2
0.50	-7.3
0.30	-0.2
-0.20 (In-direction Motion)	+0.6

simulation results, the maximum drag force is applied on the robot in the pipelines with 100 kPa and 1.2 m/s relative velocities and the amount of drag force is around 26 N. Since the geometry of the robot is symmetric, each motor is needed to provide around 8.7 N to overcome this force. We characterize the gear-motor, spring mechanism, and battery capacity to have a fully automotive system in extreme operating conditions.

2.3.3. Gear-motor

Based on the maximum required traction force for the motor in the extreme operation condition and the radius of the wheels (i.e. 5 cm), and also the rather high velocity levels we desire for the robot, a customized hear-motor is selected from Maxon Motors Inc©. The selected gear-motor is equipped with an incremental encoder that measures the angular velocity of the gear-motor. Table 2.3 shows the characteristics of the customized gear-motor.

Table 2.3. Specification of the Motor (DCX22l), the Gearhead (GPX22UP) and the Encoder (ENX 16 Easy).

Specification [unit]	Value
Nominal Voltage [V]	12
Diameter [mm]	22
Length [mm]	92
Nominal Torque at Motor Shaft [mN.m]	791
The Reduction Ratio of the Gearhead	26:1
Number of Motors in the Robot	3
# of Counts Per Turn for the Encoder	26624
# of Channels in the Encoder	3

2.3.4. Spring Mechanism Characterization

The objective of the spring characterization is to find a value for stiffness of the spring that ensures reliable pressing force for the robot. In this section, the problem is formulated based on the robot geometry and maximum traction force that each wheel needs to provide.

A wheeled-robot has controlled motion if its wheels have absolute rolling on the surface. To this aim, the maximum traction force generated at the contact area needs to be less than the maximum friction force between the pipe and the wheel:

$$F_{T(max)} \leq f_{s(max)} \tag{2.1}$$

where $F_{T(max)}$ is the maximum traction force and $f_{s(max)}$ is the maximum friction force. Our robot is considered symmetric and the wheels below its geometric center bear the weight of the robot in which the weight of the robot increases the contact force, F_N (see figure 2.7a). Hence, the required stiffness for the associated spring for them is less. To calculate the maximum spring force, we consider the wheel that is above the center of mass and provides F_N' (see figure 2.7a). Also, we

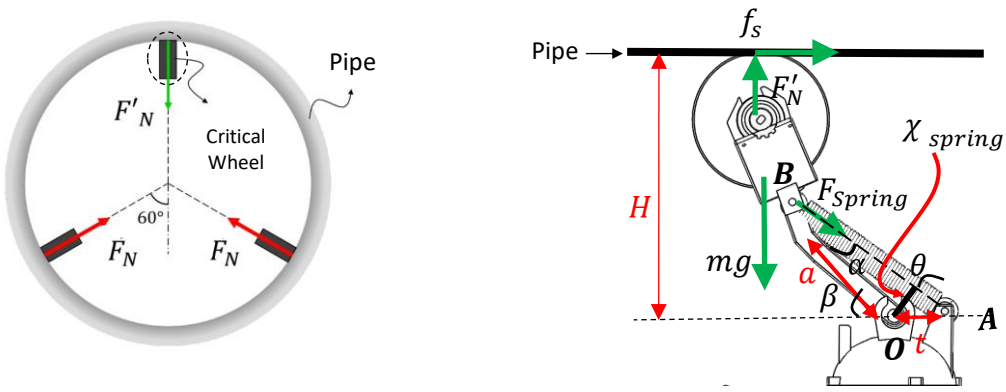

(a) (b)

Figure 2.7. (a) Free Body Diagram of the Robot. (b) Static Force Analysis for the Wheel.

consider all the weight of the robot on one wheel and perform static force analysis for it (see figure 2.7a). Also, all the weight of the robot is considered at the pipe wheel contact. In figure 2.7b, the free body diagram of the arm is shown. If the central processor remain at the center of the pipe (which is the required criterion), the static force analysis on point ***O*** can be written as [75]:

$$\sum M_{\boldsymbol{O}} = 0 \rightarrow (mg - F'_N)a\cos\beta = f_s.H + F_{Spring}\,\chi_{Spring} \tag{2.2}$$

Based on ***OAB*** triangle, we can write:

$$\beta = \alpha + \left(\frac{\pi}{2} - \theta\right) \tag{2.3}$$

$$\alpha = \sin^{-1}\left(\frac{t}{a}\cos\theta\right) \tag{2.4}$$

Plugging (2.4) into (2.3):

$$\beta = -\theta + \sin^{-1}\left(\frac{t}{a}\cos\theta\right) + \frac{\pi}{2} \tag{2.5}$$

On the other side, we have:

$$\beta = \sin^{-1}\left(\frac{H}{L}\right) \tag{2.6}$$

Considering (2.5) and (2.6), we have a nonlinear trigonometric equation that θ (see figure 2.7b) is calculated based on the pipe radius, H. We also can write:

$$\chi_{Spring} = t\cos\theta \tag{2.7}$$

Plugging (2.5), (2.6), (2.7) into (2.2), we can write the spring force, F_{Spring}, as:

$$F_{Spring} = \frac{1}{t\cos\theta}\left((F_N' - mg)a\cos\left(\theta + \sin^{-1}(\frac{t}{a}\cos\theta)\right) - f_s H\right) \tag{2.8}$$

The springs are linear in which the force is proportional to its displacement. Hence, based on the geometry of the anchor points (***A*** and ***B*** in figure 2.7b), the initial length of the spring has no pretension at $\theta = 0$ and is calculated as $\sqrt{(t+\cos\beta)^2 + (a\sin\beta)^2}\ \cos\theta$. The length of the spring at $\theta > 0$ is calculated as $\sqrt{(t+\cos\beta)^2 + (a\sin\beta)^2}$. K is the spring stiffness and F_{Spring} is calculated as:

$$F_{Spring} = K\left(\sqrt{(t+\cos\beta)^2 + (a\sin\beta)^2}\right)(1-\cos\theta) = KU(\theta) \tag{2.9}$$

The value for a= 4.05-in and t =1.42-in. Plugging (2.9) into (2.8), K is calculated as:

$$K = \frac{1}{t\cos\theta(U(\theta))}\left((F_N' - mg)a\cos\left(\theta + \sin^{-1}(\frac{t}{a}\cos\theta)\right) - f_s H\right) = G(\theta) \tag{2.10}$$

The appropriate value for K is the maximum of the (2.10), Hence:

$$K = max(G(\theta)) \tag{2.11}$$

The maximum traction force computed with the CFD work in SolidWorks is considered for f_s that is 8.7 N based on (2.1) for each wheel. Also, for H, the values that the robot can cover are considered (4.5 in$\leq H \leq$11in). The friction between pipe and wheel contact is considered dry coulomb friction force. Hence, the relation between F_N' and $f_{s(max)}$ is:

$$f_{s(\max)} = \mu_s F_N' \tag{2.12}$$

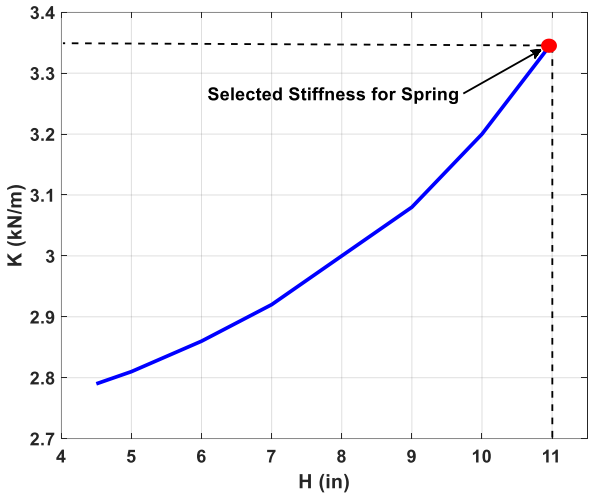

Figure 2.8. Stiffness Value Calculation for Pure Rolling of the Wheels.

In (2.12), μ_s is the friction coefficient and is considered 0.8 based on [75]. Hence, the value for F'_N is calculated ≈11N. In figure 2.8, different values for K that ensure pure rolling for wheels in different pipe diameters are shown. To cover all pipe diameters, the maximum value in figure 2.8 is selected (i.e. 3.34 kN/m). Hence in all pipe sizes, the friction force is sufficient for pure rolling of the wheels that results in a controlled motion for the robot inside the pipe.

2.3.5. Power Consideration

In this section, we propose a recursive method to calculate the minimum battery capacity and operation duration for the robot based on the maximum drag force that we calculated in the extreme operation condition. In this methodology, we consider that the main power consumers in our robot are gear motors and other components like wireless communication systems consume negligible power compared to gear-motor. We consider gear motors for power profiling. First of all, we assume an operation duration, h for the robot with one turn of battery charge. Based on the

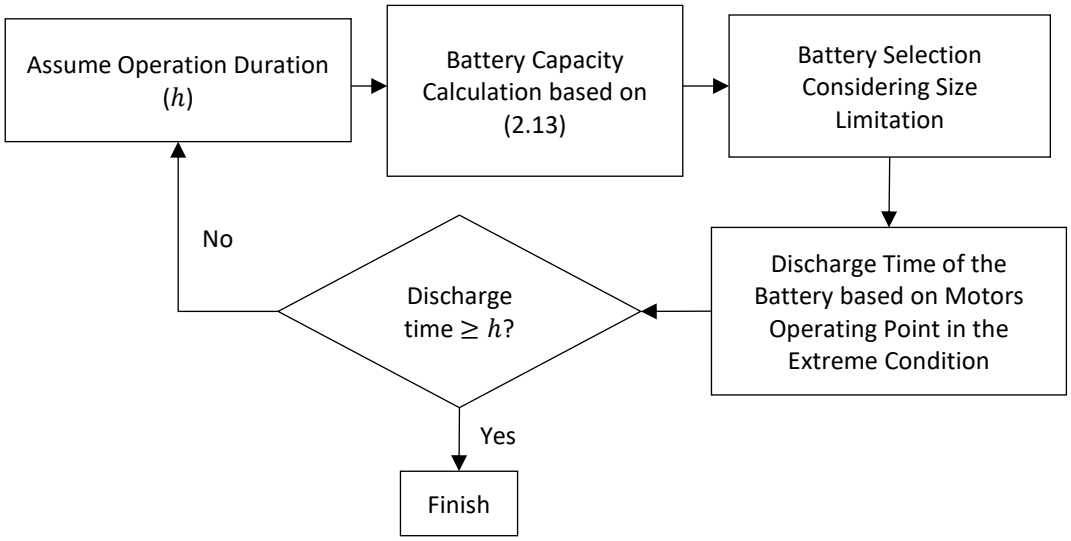

Figure 2.9. Recursive Approach to Calculate Minimum Battery Capacity.

properties of the selected gear-motors (power and nominal voltage), and also the number of motors in the robot, the minimum battery capacity is calculated as follows:

$$C = \frac{3P.h}{V_n} \tag{2.13}$$

In (2.13), C (A.h) is battery capacity, h (hour) is operation duration, P (W), and V_n (V) are the gear-motors' power and nominal voltage, respectively. Factor three in (2.13) accounts for the number of motors in the robot. Afterwards, a commercial-off-the-shelf (COTS) battery considering size limitations in the robot is selected. The discharge time of the battery is defined based on the battery characteristics (i.e. defined in the battery's datasheet), and the drawn electrical current by the gear motors. The amount of the drawn current is calculated based on the maximum torque the gear-motors are required to provide in the extreme condition (i.e. calculated in the CFD simulation). The process is repeated until the operation duration and the discharge time are approximately equal (Figure 2.9). We calculated the minimum battery capacity to be 15A.h, and the operation duration of the robot is 3 hours in the extreme operating condition.

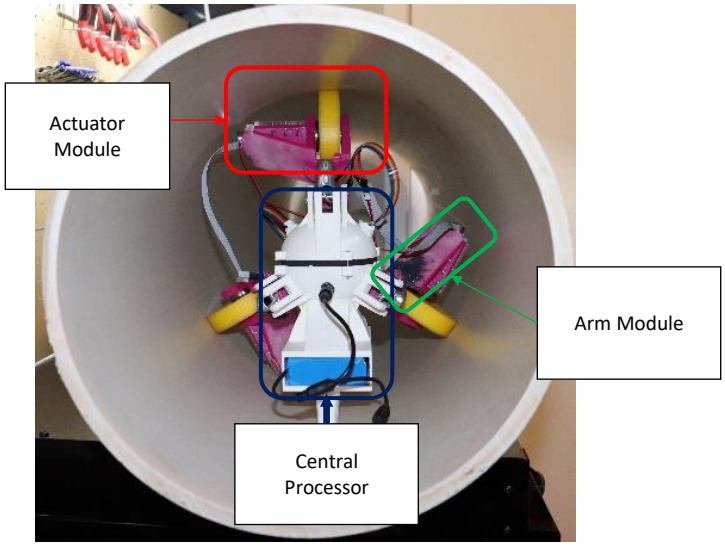

Figure 2.10. Prototype of the Robot.

2.4. Robot Prototyping

The prototype of the robot is shown in figure 2.10. The designed components in SolidWorks are manufactured using 3D printing technique by ABS material. The stiffness of the off-the-shelf passive spring is higher than the calculated stiffness due to the available springs in the market. The battery is isolated in the battery-case by moldable glue. The battery has additional cable that recharges the battery. The wires of the gear-motors and encoders are directed to the central processor by two sealed holes. The pins that connect the springs to the central processor and arms are 52100 alloy steel with 0.75 in diameter and are corrosion-resistant. We measured the maximum velocity of the robot along the pipe axis ≈1.56 m/s in the initial experiments to evaluate the motion functionality of the robot. Also, the robot can move in the vertical direction with maximum velocity 0.9 m/s. The prototype has 2.23 kg weight that is much lighter than similar counnterparts (e.g. PipeDiver [12] and PureRobotics [76] from Pure Technologies Inc©). This feature of the robot (i.e. being lightweight) decreases the cost of launching system that is used to insert and extract the robot from the pipeline network. Figure 2.11a-b show the launching system

(a) (b)

Figure 2.11. Launching System for (a) PipeDiver. Adapted from [12]. (b) PureRobotics. Adapted from [76].

for PipeDiver and PureRobotics that are large and add to the cost of operation. In addition, since these robots are rather large, an access point needs to be created in the pipe to insert the robots into the system. Based on the industry interview, it is highly desired to insert and extract the robot from the available manholes and access points that already exist in the network and our robot has this potential. Table 2.4 lists the specifications of the robot.

Table 2.5. The Specifications of the Robot Prototype.

Parameter [unit]	Value
Size Adaptability Range [in]	9-22
Length [in]	7.5-9
Maximum Linear Speed [m/s]	1.56
Vertical Motion Capability	Yes
Weight [kg]	2.23

2.5. Notes and References

In this chapter, we designed a modular and size adaptable in-pipe robot. The robot is maneuverable with one set of actuator modules that can is used for both driving and steering. In our design, we accomplished greater agility (i.e. 1.56 m/s in horizontal paths) and maneuverability (i.e. size-adaptable and rotation around two non-pipe axes) for the robot compared to similar works [29], [34]–[36], [38], [77]. In this design, we achieved wider size-adaptability range compared to current works [16], [27], [28], [30], [36], [38], [39], [41]. The majority of in-pipe robots are powered by cable [33]–[36], [41], [77] and among the battery-operated robots, [16], [71], operation condition is not considered. We are the first to design a battery-operated robot considering the operating conditions and achieved longer operation duration in in-service network. We considered the requirements toward the design of a resilient machine [72]. The requirements in our applications are spring mechanism characterization and battery capacity to ensure a reliable motion in pipelines during operation.

3. MOTION CONTROL ALGORITHM FOR THE ROBOT*

3.1. Introduction

Distribution systems (Figure 3.1 [1]) comprise pipelines with different configurations. The robot experiences change in pipe diameter during operation, there is high-velocity flow in which applies huge disturbance on the robot. Aging pipes have non-circular and uncertain shapes due to sediments and corrosion. The robot needs to track a desired velocity in pipelines and steer to desired direction at non-straight configurations like 90-degree bends or T-junctions. Hence, motion controller is needed to handle these uncertainties and disturbances and enables the robot to steer to desired direction at non-straight configurations.

The design of the robot is inspired by under-actuated two-wheeled inverted pendulum systems [78] [79]. Under-actuated design is useful for our application since we can save power and space as the number of control inputs (of actuators) is fewer than the degree-of-freedom (DOF) in these type of systems. On the other hand, motion controller for these robots are more sophisticated than the controllers for actuated systems due to redundancy in under-actuated systems [79]. In addition, there are uncertainty and disturbance in operating environment of the robot (i.e. pipelines) and also

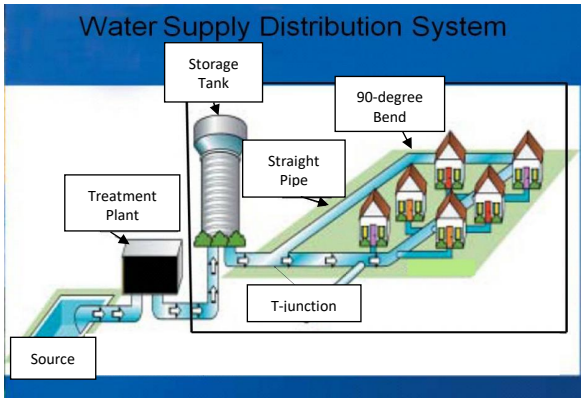

Figure 3.1. A Typical Water Distribution System. Source: Adapted from [1].

*Part of the data reported in this chapter is reprinted with permission from "An LQR-assisted Control Algorithm for an Under-actuated In-pipe Robot in Water Distribution Systems" by Saber Kazeminasab, Roozbeh Jafari, M. Katherine Banks, SAC '21: Proceedings of the 36th Annual ACM Symposium on Applied Computing, pp. 811-814, Copyright 2021 by ACM Digital Library.

the pipelines comprise complicated configurations that makes reliable motion of the robot challenging.

In this chapter, we develop three phases of motion control algorithm to address the challenges of motion of the robot in pipes. The motion controller is not integrated and instead, we designed three phases in which in each phase, a specific requirement for motion is satisfied. In junctions, the robot needs to stop with stabilized configuration and to this aim, we develop a stabilizer controller based on a linear quadratic regulator (LQR). Also, the robot is required to steer the robot to desired paths with reliable motion at junctions, and to this aim, we design a controller that facilitates rotation around two axes with desired amount of rotation for the robot. In straight path, the robot is required velocity tracking with stabilized configuration and to this aim, we design a controller that stabilizes the robot in pipe and enables it to track a desired velocity.

We first model the robot with its dynamical equations and then design the three phases of the controllers and evaluate their functionality with simulation and experimental results.

3.2. Robot Modelling

Figure 3.2a shows the free body diagram of the robot in pipe that has an inclination angle with respect to the horizontal surface (i.e. α). $\dot{x}$, ϕ, and ψ are linear velocity of the robot along pipe axis, rotation around the y-axis, and rotation around the z-axis. Since the stiffness of springs is high, it is assumed that the robot does not have linear motion on the y-axis and z-axis, and the rotation around the x-axis is assumed zero. The traction forces of the wheels (i.e. F_1, F_2, and F_3) are generated by gear-motors (i.e. $F_i = \frac{\tau_i}{R}, i = 1,2,3$). we have:

$$\frac{\tau_1}{R} + \frac{\tau_2}{R} + \frac{\tau_3}{R} - mg\sin(\alpha) - \frac{1}{2}\rho A C_D(\dot{x} - V_f)^2 = m\ddot{x} \tag{3.1}$$

where m, C_D, ρ, and A are the robot's mass, drag coefficient, water density, and cross-sectional area of the robot facing water flow [73]. The term $\frac{1}{2}\rho A C_D(\dot{x} - V_f)^2$ is the drag force that applied

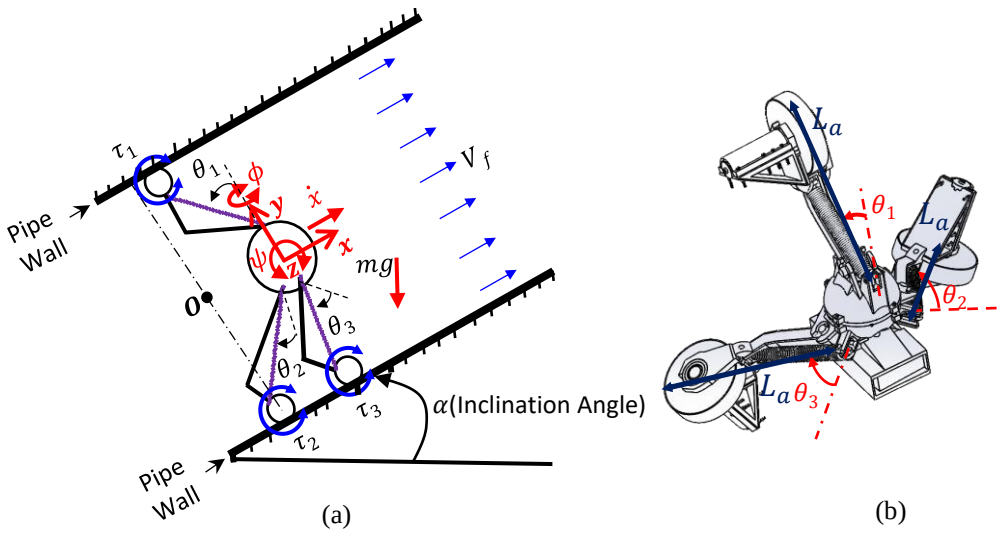

Figure 3.2. (a) Free Body Diagram of the Robot. (b) Arm Angles (θ_1, θ_2, and θ_3).

to the robot due to relative velocity between the robot and water flow (i.e. $\dot{x} - V_f$). The analysis of dynamical torque with respect to ***O*** (Figure 3.2a) is written as:

$$\frac{\tau_3}{2R} L_a \cos(\theta_3 - \phi) - \frac{\tau_2}{2R} L_a \cos(\theta_2 + \phi) = I_{yy}\ddot{\phi} \tag{3.2}$$

$$\frac{\sqrt{3}\tau_3}{2R} L_a \cos(\theta_3 - \phi)\,(1 + \sin\psi) + \frac{\sqrt{3}\tau_2}{2R} L_a \cos(\theta_2 + \phi)(1 + \sin\psi) - \frac{\tau_1}{R} L_a \cos(\theta_3 + \psi) -$$

$$mgL_a \sin(\theta_1 + \psi) = I_{zz}\ddot{\psi} \tag{3.3}$$

Table 3.1 presents the parameters in the dynamical equations of the robot. In (3.1)-(3.3), τ_i, R, and i are motor torque, wheel radius, and the wheels numbers, respectively. The motor torque (τ) is linearly computed with electrical current pass through it. We can express the governing equation of the gear mottos with the following set of equations:

Table 3.1. Specification of the Robot in Dynamic Analysis.

Parameter [unit]	Description	Value
θ_1	Arm #1 Angle	Variable
θ_2	Arm #2 Angle	Variable
θ_3	Arm #3 Angle	Variable
L_a	Arm Length	17cm
m	Robot Mass	2.23 kg
I_{yy}	Robot's Moment of Inertia around the Y-axis	0.0126kg.m^2
I_{zz}	Robot's Moment of Inertia around the Z-axis	0.0093kg.m^2
ϕ	Robot's Rotation Angle around the Y-axis	Variable
ψ	Robot's Rotation Angle Around Z-Axis	Variable
F_1	The Traction Force Of Actuator #1	Variable
F_2	The Traction Force Of Actuator #2	Variable
F_3	The Traction Force Of Actuator #3	Variable
F_d	Drag Force	Variable
τ_1	Torque of gear-motor #1	Variable
τ_2	Torque of Gear-motor #2	Variable
τ_3	Torque of Gear-motor #3	Variable
R	Wheel Radius	5cm
D	Pipe Diameter	Variable
V_f	Flow Velocity	Variable
$\dot{x}$	Robot Velocity	Variable

$$\begin{gathered} \frac{v_{co}}{L_m} - \frac{v_e}{L_m} - \frac{R_m}{L_m} i_m = \frac{di_m}{dt} \\ v_e = K_v \dot{\vartheta} \\ \tau_m = K_v i_m \\ \frac{n^2}{I_l + n^2 I_R} \tau_m = \ddot{\vartheta} \end{gathered} \tag{3.4}$$

Table 3.2. Parameters in Gear-Motors Dynamical Equations.

Parameter [unit]	Description
v_{co}[V]	Applied Voltage on the Motor
v_e [V]	Back EMF Voltage
i_m [A]	Current Pass Through Motor
K_v $[min^{-1}.V^{-1}]$	Speed Constant
$L_m[H]$	Terminal Inductance
$R_m[\Omega]$	Terminal Resistance
$\dot{\vartheta}$[rad/s]	Shaft Angular Velocity
$\ddot{\vartheta}$[rad/s^2]	Shaft Angular Acceleration
n	Gear Reduction Ratio
I_l[kg.m^2]	Load Inertia
I_R[kg.m^2]	Rotor Inertia

The parameters in (3.4) are described in Table 3.2.

3.3. The Controller at Junctions (Phase 1)

Our goal in stabilization is to locate the central processor of the robot at the center of pipe during operation. State-feedback controllers are good candidates for this aim [79]. We need state-space representation of our system to design the state feedback controller while the governing dynamical equations of the system are nonlinear. We linearize the equations of the robot to this aim, the equations are decoupled into two sets: One set is related to the linear motion of robot, (i.e. 3.1), and the other set is related to the orientation of the robot (i.e. (3.2) and (3.3)). $x_s(t) = [\phi \quad \dot{\phi} \quad \psi \quad \dot{\psi}]^T$ are considered as stabilizing states (see Figure 3.3) that need to be kept at zero value during operation. We linearized (3.2) and (3.3) around the equilibrium point that is $x_s^e = [0 \quad 0 \quad 0 \quad 0]^T$ and derived system's auxiliary matrices. We have:

$$x_s = \begin{bmatrix} x_1 = \phi \\ x_2 = \dot{\phi} \\ x_3 = \psi \\ x_4 = \dot{\psi} \end{bmatrix} \tag{3.4}$$

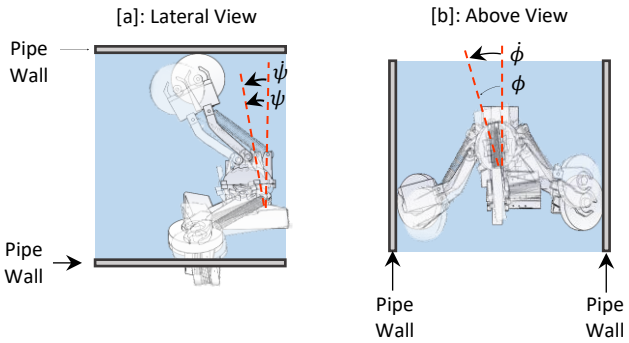

Figure 3.3. Stabilizing States for the Robot.

$$u = \begin{bmatrix} u_1 = \tau_1 \\ u_2 = \tau_2 \\ u_3 = \tau_3 \end{bmatrix} \tag{3.5}$$

$$\dot{x}_s = F(\theta_1, \theta_2, \theta_3, \phi, \psi, u) = \begin{bmatrix} F_1 \\ F_2 \\ F_3 \\ F_4 \end{bmatrix} \tag{3.6}$$

where $F_1 = x_2$, $F_2 = \frac{1}{RI_{yy}}[\frac{\sqrt{3}}{2}\tau_3 L_a \cos(\theta_3 - \phi) - \frac{\sqrt{3}}{2}\tau_2 L_a \cos(\theta_2 + \phi)]$, $F_3 = x_4$, and $F_4 = \frac{1}{I_{zz}}[\frac{1}{2R}\tau_3 L_a \cos(\theta_3 - \phi) + \frac{1}{2R}\tau_2 L_a \cos(\theta_2 + \phi) - \frac{1}{R}\tau_1 L_a \cos(\theta_1 + \psi) - mg \sin(\theta_1 + \psi)$. We have:

$$A_s = \begin{bmatrix} \frac{\partial F_1}{\partial x_1} & \frac{\partial F_1}{\partial x_2} & \frac{\partial F_1}{\partial x_3} & \frac{\partial F_1}{\partial x_4} \\ \frac{\partial F_2}{\partial x_1} & \frac{\partial F_2}{\partial x_2} & \frac{\partial F_2}{\partial x_3} & \frac{\partial F_2}{\partial x_4} \\ \frac{\partial F_3}{\partial x_1} & \frac{\partial F_3}{\partial x_2} & \frac{\partial F_3}{\partial x_3} & \frac{\partial F_3}{\partial x_4} \\ \frac{\partial F_4}{\partial x_1} & \frac{\partial F_4}{\partial x_2} & \frac{\partial F_4}{\partial x_3} & \frac{\partial F_4}{\partial x_4} \end{bmatrix} \tag{3.7}$$

$$B_s = \begin{bmatrix} \frac{\partial F_1}{\partial u_1} & \frac{\partial F_1}{\partial u_2} & \frac{\partial F_1}{\partial u_3} \\ \frac{\partial F_2}{\partial u_1} & \frac{\partial F_2}{\partial u_2} & \frac{\partial F_2}{\partial u_3} \\ \frac{\partial F_3}{\partial u_1} & \frac{\partial F_3}{\partial u_2} & \frac{\partial F_3}{\partial u_3} \\ \frac{\partial F_4}{\partial u_1} & \frac{\partial F_4}{\partial u_2} & \frac{\partial F_4}{\partial u_3} \end{bmatrix} \tag{3.8}$$

Auxiliary matrices are calculated by substituting x_s^e and u_e in (3.7) and (3.8) where u_e is the controller input at the equilibrium point. $C_s = \begin{bmatrix} 0 & 1 & 0 & 0 \\ 0 & 0 & 1 & 0 \end{bmatrix}$ is the system's output matrix. The system's auxiliary representation in state-space form is:

$$\begin{aligned} \dot{x}_s &= A_s x_s + B_s u \\ y_s &= C_s x_s \end{aligned} \tag{3.9}$$

following onwards, we design the state feedback-based LQR controller [80]. To this aim, we define a cost function:

$$J(K) = \frac{1}{2}\int_0^\infty [x_s^T Q x_s + u^T R u] dt \tag{3.10}$$

where Q weights x_s and R weights u. The cost function, $J(K)$, depends on $K$and is minimized when K is:

$$K = R^{-1} B_s^T P \tag{3.11}$$

where P is calculated with algebraic Riccati equation [79]:

$$-PA_s - A_s^T P - Q + PB_s R^{-1} B_s^T P = 0 \tag{3.12}$$

K is then used to calculate the LQR stabilizer's output, u, that is:

$$u = -Kx_s \tag{3.13}$$

The proposed LQR controller keeps $x_s(t)$ at the equilibrium point (i.e. x_s^e) that results in the central processor to remain at the center of pipe during operation. The observer in the proposed controller

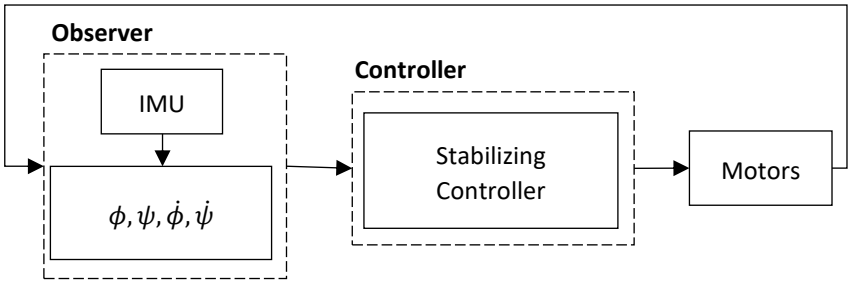

Figure 3.4. Stabilizer Controller in Junctions.

Table 3.3. Specifications of the Experiments for the Stabilizer Controller.

Iteration #	Initial Value for ϕ (ϕ_0) (degree)	Initial Value for ψ (ψ_0) (degree)
1	-46	-37
2	-25	-21
3	+22	+46
4	+15	+18

includes an inertial measurement unit (IMU) which comprises an accelerometer and gyroscope. The output of the IMU sensor is noisy and to have reliable output from the IMU, we used Mahony filter [81] to calculate ϕ and ψ (i.e. orientation of the robot). Mahony filter computes the orientation of the robot by fusing data from the accelerometer and gyroscope of the IMU. $\dot{\phi}$ and $\dot{\psi}$ are provided directly by the gyroscope. The controller in this phase is shown in figure 3.4. The performance of the controller in this phase is evaluated with experimental results. In the experiment, BMI160 which is a 6-DOF accelerometer and gyroscope is used as IMU and located on the central processor and the robot is located in a 14-in diameter pipe. The experiment is

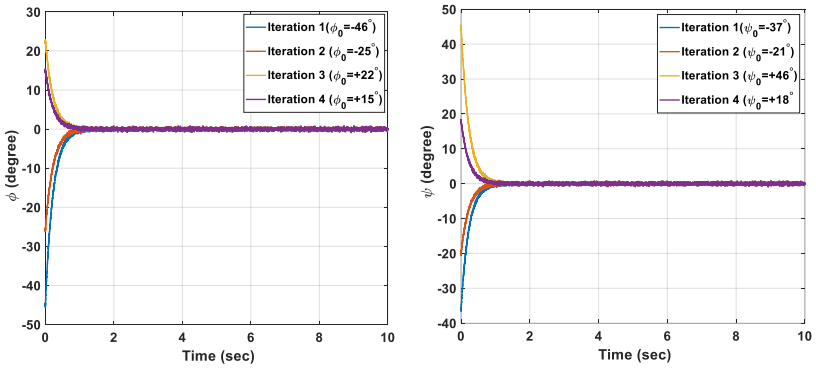

Figure 3.5. Performance of the Stabilizer Controller. (a) ϕ. (b) ψ.

repeated in four iterations in which in each iteration, an initial deviation for ϕ and ψ are given to the robot (see table 3.3) and the controller is expected to cancel (i.e. bring them to zero) the deviations. The results in figure 3.5 show that the initial deviations are canceled within one second since the motion is started and the stabilizing states are kept at zero in the rest of the motion. Hence, the controller can cancel the deviations within one second.

3.4. The Controller in Straight Path (Phase 2)

The robot needs to track desired linear velocity along pipe axis in addition to the stabilization in straight path. To this aim, we design a velocity controller and combine it with the stabilizer controller that was developed in phase 1 (in section 3.4). Since the wheels of the robot have absolute rolling on pipe wall, linear velocity of the robot is directly computed from the angular velocity of the wheels (if all three wheels have approximately equal angular velocity). The relation between the linear velocity and the angular velocity of the wheels can be written as:

$$v \approx R\omega \tag{3.14}$$

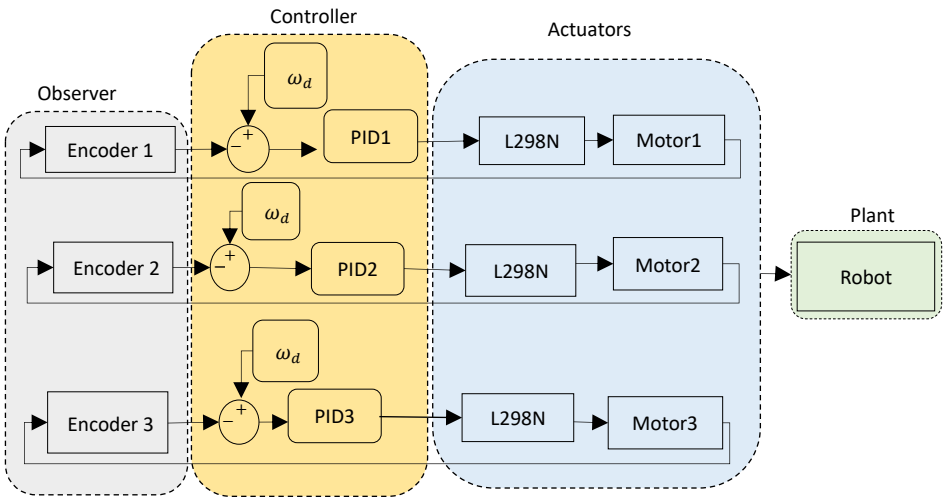

Figure 3.6. Velocity Controller for the Robot. ω_d: Reference Velocity for the Wheels.

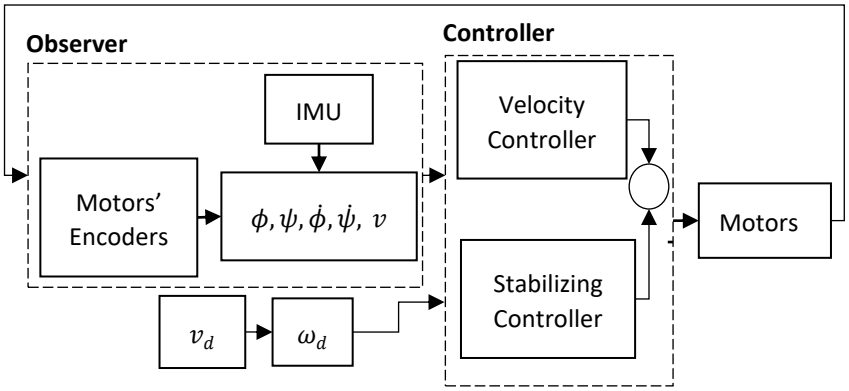

Figure 3.7. Phase 2 of the Controller for the Robot.

where v is the linear velocity and ω is the angular velocity of the wheels. The desired angular velocities of the wheels, ω_d is computed by desired linear velocity, $\boldsymbol{v_d}$. In the velocity controller (see figure 3.6), the gear-motors' encoders measure the angular velocity of the wheels. Three proportional-integral-derivative (PID) controllers control the velocity of the wheels. L298N in figure 3.6 is gear-motor driver in which amplifies the control signal from the microcontroller to power signal to drive the gear-motors. We combined the velocity controller and the stabilizer to have the stabilizer-velocity tracking controller in phase 2 that is shown in figure 3.7 and controls the motion of the robot in straight paths. The observer in this controller includes the IMU and three motor encoders. We evaluated the performance of this controller with experiment. The experiment is repeated in four iterations and in each iteration, initial deviations for stabilizing states and desired

Table 3.4. Specifications of the Experiments for the Stabilize-velocity Tracking Controller.

Iteration #	Desired Velocity (m/s)	Initial Value for ϕ (ϕ_0) (degree)	Initial Value for ψ (ψ_0) (degree)
1	0.10	+14	-23
2	0.20	-13	+31
3	0.30	-9	-18
4	0.35	-4	+22

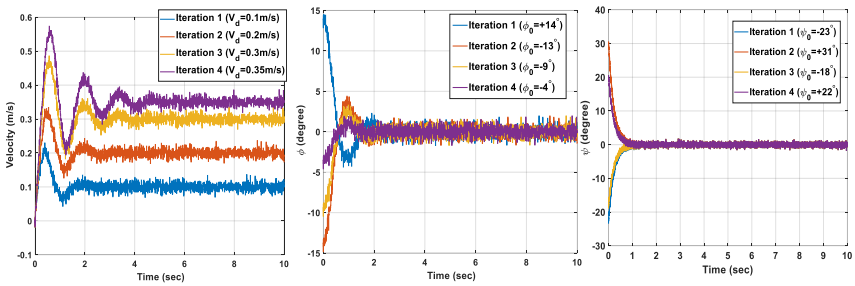

(a) (b) (c)

Fig. 3.8. Performance of the Stabilizer-velocity Tracking Controller. (a) Linear velocity (b) ϕ (c) ψ

linear velocity for the robot are considered (see Table 3.4). The experimental results in figure 3.8 show that the initial deviations are canceled within two seconds since the motion is started and the robot reaches desired velocity within four seconds (on average) of the motion start. Hence the proposed controller in a straight path fulfils the requirements of motion in a straight path that are moving with the desired velocity with stabilized configuration.

3.5. Controller at Non-straight Configurations (Phase 3)

The robot needs to steer to the desired direction at non-straight configurations of pipelines. To this aim, we design a controller that facilitates a desired amount of rotation at junctions around y and z axes with differential drive motion. In other words, the rotation for the robot is facilitated by assigning different desired angular velocities to the wheels (ω_{1d}, ω_{2d}, and ω_{3d}). Figure 3.9 shows

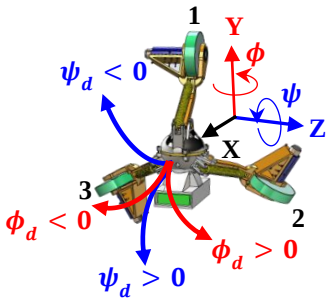

X-axis: Pipe Axis

Figure 3.9. Coordinate System on the Robot and Differential Motion Definition.

Table 3.5.5. Desired Angular Wheels Motion in Various Differential Motions.

Differential Motion Type	Desired Velocity for Wheel 1 (ω_{1d})	Desired Velocity for Wheel 2 (ω_{2d})	Desired Velocity for Wheel 3 (ω_{3d})
$\phi_d > 0$	0.5 (Maximum Velocity + Minimum Velocity)	Minimum Velocity	Maximum Velocity
$\phi_d < 0$	0.5 (Maximum Velocity + Minimum Velocity)	Maximum Velocity	Minimum Velocity
$\psi_d > 0$	Minimum Velocity	Maximum Velocity	Maximum Velocity
$\psi_d < 0$	Maximum Velocity	Minimum Velocity	Minimum Velocity

the definition of differential motion for the robot and Table 3.5 lists the desired velocities for the wheels in each differential motion. The maximum and minimum in Table 3.5 stand for unequal velocities (where maximum velocity is greater than minimum velocity) and their value is defined based on the desired linear speed at passing the non-straight configuration. The controller is shown in figure 3.10 and includes a trajectory generator, an observer, an error-check submodule, and three velocity controllers. The observer in the controller provides information about the orientation and angular velocities of the wheels ($\omega_1, \omega_2, \omega_3$), and the error-check sub-module monitors the status of rotation (of the robot) during rotation. To evaluate the performance of the robot and the controller in non-straight configurations (phase 3), we do ADAMS/MATLAB co-simulation. ADAMS is a dynamic simulation software and can model the parameters of the robot and the

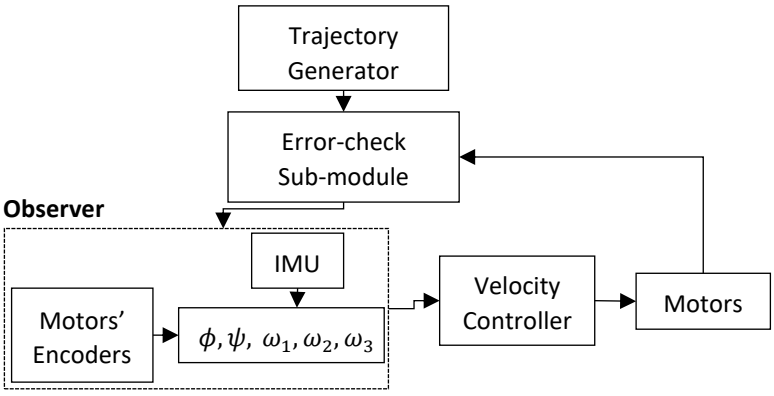

Figure. 3.10. Phase 3 of the Controller.

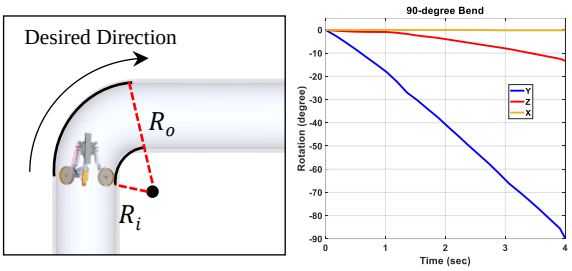

(a) (b)

Figure 3.11. (a) Desired Direction in a Bend. (b) Amount of Rotation Around Axes.

operating environment of the robot inside pipe. The robot and pipe are simulated in ADAMS and the developed controller is implemented in the MATLAB Simulink toolbox. We evaluate the performance of the controller in phase 3 in bends and T-junctions in which are common non-straight configurations in pipelines.

3.5.1. Controller Performance at 90-degree Bend

In this part, the performance of the robot and the controller in bends is validated. The robot is supposed to track the desired direction in figure 3.11a in which it needs to rotate 90° clockwise around the y-axis ($\phi_d = -90°$). The inner radius of the bend, R_i, is 12-in and the outer diameter, R_o, is 24-in. The desired linear speed is 10 in/s and the desired angular velocities for the wheels are: $\omega_{1d} = 34.5$ rpm, $\omega_{2d} = 46$ rpm, and $\omega_{3d} = 23$ rpm. The amount of rotation around axes at the end of the motion is shown in figure 3.11b that shows complete rotation around the desired axis (y-axis) with small rotation around the x-axis ($\approx -0.66°$) and z-axis ($\approx -13.33°$) at the end motion. The rotation around the x-axis is almost zero as expected. We repeated our simulations and validated that the robot and the controller can cover the bends with diameters ranging from 9-in to 22-in.

3.5.2. Controller Performance at T-junction

The robot is supposed to track the desired direction shown in figure 3.11a (i.e. the amount of

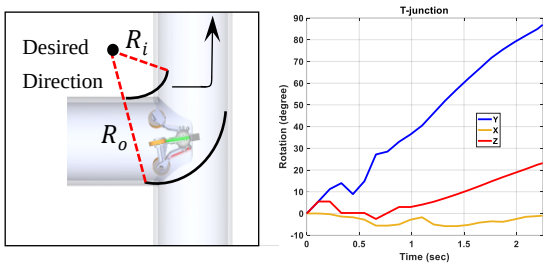

(a) (b)

Figure 3.12. (a) Desired Direction in T-junction. (b) Amount of Rotation Around Axes.

rotation is 90° counter-clockwise (i.e. $\phi_d = +90°$)). R_i, is 14-in and R_o is 28-in. The desired linear speed is around 15 in/s and the desired angular velocities for the wheels are: $\omega_{1d} = 73$ rpm, $\omega_{2d} = 49$ rpm, and $\omega_{3d} = 97$ rpm. The amount of rotation at the end motion around each axis shows complete rotation around the desired axis with small rotation around the x-axis ($\approx -1.21°$) and z-axis ($\approx +22.46°$) (Figure 3.12b) that are canceled when the robot switches to stabilizer-velocity tracking controller. We repeated our simulations and derived the T-junction coverage to be 9-in and around 15-in. In our simulations, we found that the inner radius shape of the T-junction plays an important role in reliable motion. The stiffer the inner shape of the T-junction, the less reliable motion. However, the pretension in the springs makes the arms stick to the pipe wall, but it leads to rotation around the x-axis that is undesirable and the coordinate system needs to be updated. The rotations around the z-axis can be canceled when the robot switched to the stabilizer-velocity tracking phase.

3.6. Notes and References

In this section, we designed a multi-phase motion control for our proposed robot that enables maneuverability with stabilized motion in complicated configurations of pipeline that is has been a challenge for in-pipe robots [16], [38], [41], [47], [49], [50], [71], [82]–[84]. However, switching between different phases of motion controllers remains a challenge to solve. In other words, the robot needs to localize itself in the network to choose the appropriate phase of the motion controller. In the next section, we propose a method that enables the robot to localize itself during operation and navigate through complicated configurations of pipelines.

4. WIRELESS COMMUNICATION AND EMBEDDED SYSTEM DESIGN*

4.1. Introduction

There are different ways that an in-pipe robot can communicate with the base station; it can store sensor measurements on an SD card [12], transmit them with wire [77], or wirelessly [57] during operation. However, the first two methods are not feasible in long-distance traveling of the in-pipe. In storing method, it is not possible to localize the robot inside pipeline that results in the possibility connection between the robot and the base station is lost. Hence, the robot is bound to straight paths in which the robot is inserted and extracted from two points in a straight line. In wired communication, the short length of cables limits the traveling length of the robot [21]. Hence, it is desired to facilitate wireless communication for in-pipe robots in which enable long-distance inspection and also provides the opportunity to localize the robot in distribution network and in this chapter, we design a wireless sensor module for the our robotic system.

In our application, the robot is equipped with a wireless system and some radio transceiver(s) are located outside the pipeline in the network. The robot switches its wireless communication between different transceivers based on its location in the network (Figure 4.1). Hence there should be easy discovery between the wireless sensor module on the robot and the transceivers outside

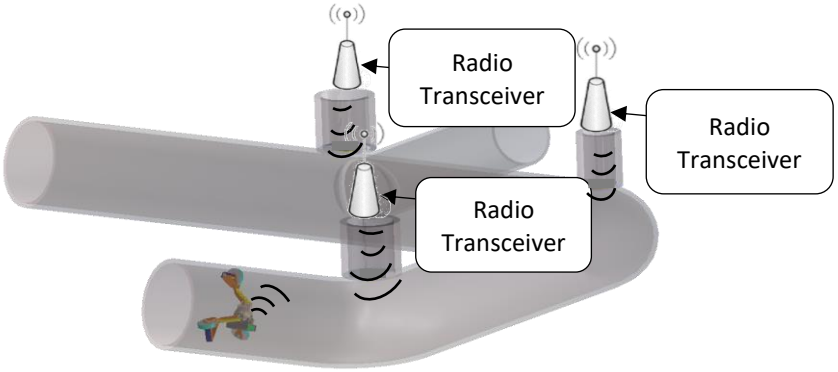

Figure 4.1. The Architecture of the Wireless Communication in Our Application.

*Part of this chapter is reprinted with permission from A Localization and Navigation Method for an In-Pipe Robot in Water Distribution System Through Wireless Control Towards Long-Distance Inspection" by Saber Kazeminasab, M. Katherine Banks. 2021. IEEE Access, pp. 117496-117511, Copyright 2021 by IEEE.

pipe. In other words, the robot and the transceivers should establish wireless communication immediately they are in range of each other. Also, we need a wireless system in which the radio signals can penetrate the harsh underground environments where signal attenuation is high [52]. In addition, in this environment, the communication link is dynamic due to variable parameters in soil; for example, the volume of water in soil affects the path loss of soil [52], [54], [85]. Also, the wireless sensor module needs to be bidirectional to facilitate sensor measurement transmission from the robot to the transceivers and motion control command transmission from the transceivers to the robot. Also, it is worth to mention that we need multi-parameter measurement and transmission which is desired based on industry interviews.

In this chapter, we design a wireless sensor module that facilitates reliable wireless communication links in few meters with high data throughput in the underground environment of pipe, soil, and water. The proposed wireless system is synchronized with: 1- the sensor module (that measures and processes sensor measurements), 2- the motion control algorithm, 3- and also the micro-pump system that provides water samples for water sensors. We evaluate the performance of the proposed wireless sensor module with experiments to investigate the reliability of the communication link in harsh environments. In our experiments, we measure the path loss model, and also validate the bi-directionality of the wireless sensor module.

In addition, we design a printed circuit board (PCB) that embeds the customized antenna of the wireless sensor module and other electronic components of the robot in the confined space of the central processor. We design the interior space of the central processor to locate the PCB and facilitate its connection with the battery that is located outside the central processor.

4.2. Wireless Communication System

In this section, we first explain the technology that we use for wireless communication, design the wireless sensor module based on the selected technology, and validate the performance of the wireless sensor module.

4.2.1. Radio Frequency Identification (RFID)

The technology we use in the wireless system for our robot is RFID. The fundamental concept of RFID systems is marking items with tags. The tags include transponders in which broadcast messages that can be read by special RFID readers. The majority of RFID tags contain a kind of identification number (i.e. tag ID) like a barcode on an item in Wal-Mart's inventory. The RFID reader decrypts information of the ID number and performs a specific task accordingly. Some RFID tags include writable memory as well that stores data for transmission to different readers (e.g. sensor measurements). RFID tags are divided into two groups: active and passive based on their power supply. Active RFID tags have a power supply that enables them to operate at greater distances while passive tags are powered by external power from the RFID reader that is coupled to the transponder by an AC field. In addition, RFID readers are divided into active and passive readers based on the tag type they read [86].

In RFID technology, seven layers of communication (i.e. open system interconnection model (OSI) [87]) are abstracted that removes the need for the synchronization of the tag and reader before data transmission. They establish communication once they are in the read range of each other [88]. Hence, communication establishment is fast that is suitable for location-sensitive applications like our application. In the environments where signal attenuation is high, signals with lower carrier frequencies can better penetrate the environment. RFID can work in low frequencies that results in better penetration in harsh environments [52], [88].

4.2.2. Bi-directional Wireless Sensor Module based on RFID in the Robot

In this research, we design a wireless sensor module based on active RFID wireless system using CC1200 from Texas Instruments (TI) Inc© as physical layer. It provides bidirectional communication link and has 128 bytes of data FIFO for both TX and RX sides. CC1200 is connected to the MCU and its functions are controlled by the MCU. Up to five sensors are connected to five analogs to digital converter (ADC) channels of the MCU and the sensor measurements are processed and located to the buffer register of the CC1200 for transmission. Next, we configure the CC1220 registers and our goal is to ensure a reliable communication link with maximum throughput. The register configuration is facilitated by the SmartRF module [89] that derives the proper value for registers based on the desired features. We configured the radio signal to have a 434 MHz carrier frequency to be able to penetrate the underground environment [52]. Also, to receive the maximum possible signal strength at the receiver side [90], we configured the maximum transmission power that CC1200 can support (i.e. 14 dBm) [91], and to have the maximum throughput, we configured the symbol rate of 1250 symbols per second (sps) and modulation format of 4-Gaussian frequency-shift keying (4-GFSK) that is the maximum throughput of CC1200 [91], [92] (see Table 4.1).

Table 4.1. Specifications of Physical Layer in Our Proposed Wireless Sensor Module.

Parameter [unit]	Description
Transceiver IC	CC1200
Carrier frequency [MHz]	434
Data Rate [kbps]	1250
Transmit Power [dBm]	14
Modulation Format	4-GFSK

4.2.3. Experimental Results

4.2.3.1. Bi-directionality

To evaluate the bi-directionality capability of the wireless sensor module to the transceiver, we performed two experiments: In the first experiment, the data packets are created in the wireless sensor modules and transmitted to the transceiver module 1. In this step, we sent 100 data packets and since an interrupt occurs on a designated pin upon reception of a data packet in transceiver module 1, it is supposed to see 100 interrupts on the pin in this experiment. We did and verified 100 interrupts on the 100 data packets on the transceiver module 1 with the logic analyzer.

In another experiment, the data packets are sent from the transceiver module 1 to the PCB and the same procedure is repeated and the same number of interrupts on the wireless sensor module's MCU and the transmitted data packets are verified. Hence, the interrupt capability of the wireless sensors module facilitates knowledge about the transmission and reception of data packets and also the number of data packets. Hence, we have a bi-directional wireless communication system in our application.

4.2.3.2. Connection Pick Capability

The robot moves in the pipe and the transceivers are located outside the pipe. We have multiple transceivers in our application (Figure 4.1) and it is important for the wireless sensor module on the robot to easily establish communication with the transceivers when it reaches the read range. To evaluate the fast discovery capability between the wireless sensor module and the transceivers, the wireless sensor module sends data packets to transceiver module 1, so we have communication between them and a graphical user interface (GUI) monitors the received packets (see figure 4.2a). During this transmission, transceiver module 2 at receive mode is added to the area and it is expected that the second transceiver also receives the same data packets as well. We

Figure 4.2. Graphical User Interface (GUI) for [a] Transceive 1, [b] Transceiver 2.

realized that transceiver 2 receives the same data packets as transceiver 1 (see figure. 4.2b). Hence, there is fast discovery between the transceivers and the wireless sensor module in this application.

4.2.3.3. Maximum Throughput of the Wireless Sensor Module

The maximum data rate in our wireless system was measured to be around 118 kbps that is greater than similar wireless underground communication systems [93]–[95] and also sufficient for wireless underground applications [52].

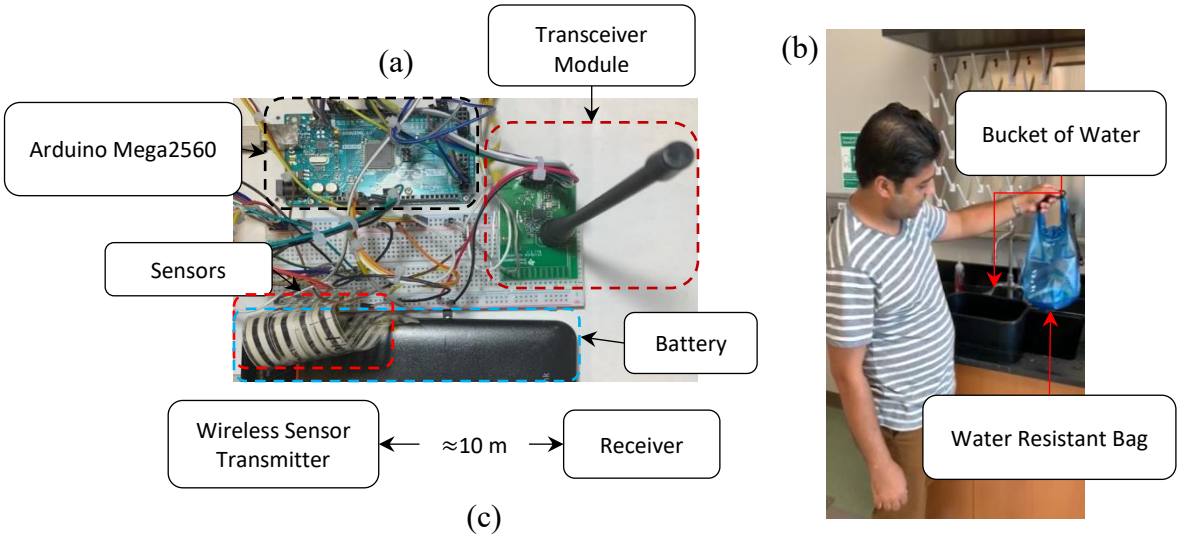

Figure 4.3. Experiment for Proof of Concept for the Proposed Wireless Sensor Module. (a) Wireless Sensor Transmitter. (b) Wireless Sensor Transmitter in PVC Bucket. c) Distance Between the Wireless Sensor Transmitter and the Receiver.

4.2.3.4. Signal Penetration of the Wireless Sensor Module in Water and Pipe Environments

In this section, we analyze the received signal strength (RSS) and data packets error (i.e. the number of packets that are received incorrectly) in the water and pipe environments. To this aim, we set an experiment in which five FlexiForce sensors are connected to five channels of the MCU, and the dynamic range of the sensors is similar to the chemical sensors. The MCU is connected to the CC1200 evaluation module and both are powered by a battery. The wireless sensor module is immersed in a bucket of water and sends the sensor measurements continuously (see figure 4.3).

Table 4.2. Experimental Results of the Proposed Wireless Sensor Module in Water and Pipe Media.

Parameter [unit]	Description
Transmitter and Receiver Distance [m]	≈10
Received Signal Strength [dBm]	-61
Packet Error [%]	0

In real application, the receiver is located above ground a few meters away from the sensor module [74], and in this experiment, we locate the transceiver ≈10 m away from the wireless sensor module and receives the data packets. A graphical user interface (GUI) offered by SmartRF Studio is connected to the reader and shows the RSS of the data packets and bit and packet errors. The average RSS in our experiments is measured -61dBm in 2 minutes duration of the experiment that is stronger than the power threshold, −100 dBm, for correct realization at receiver side [94]. Also, the bit and packet error was measured at ≈ 0% in the experiment (see Table 4.2). Hence, the wireless sensor module can penetrate the water environment with a reliable communication link.

4.2.3.5. Read Range of Wireless Sensor Module in Underground Environment

The characteristics of underground environment is highly variable in different locations. The properties of soil that affect signal attenuation (i.e. water content, temperature, soil bulk density, sand and clay composition [52]) are highly variable and each parameter has a specific impact on the communication channel (see table 4.3). Hence, the experiments in one location in soil cannot represent all situations and we need to define read range of the proposed wireless sensor module in the underground environment. To this aim, we need to provide a method to measure the read range of the wireless sensor module and also validate it with experiment. The researchers in [96] provided a numerical representation of effect of soil parameters on signal attenuation and the

Table 4.3. Soil Properties and Their Effect on Signal Attenuation. Source: Adapted from [52].

Parameter	Change	Effect on Signal Attenuation
Water Content	↑	↑
Temperature	↑	↑
Soil Bulk Density	↑	↑
% Sand	↑	↓
% Clay	↑	↑

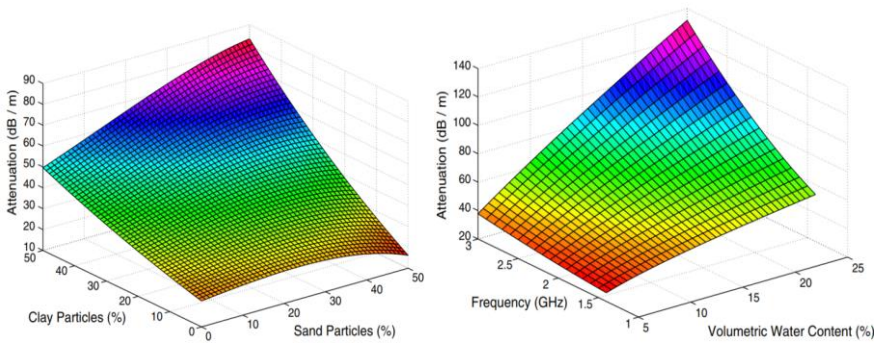

(a) (b)

Figure 4.4. (a) Signal attenuation per meter due to material absorption predicted by the model from [95] (b) Signal attenuation per meter due to material absorption predicted by the model from [95] for a soil mixture of 50% sand, 15% clay, and 35% silt. Source: Adapted from [52].

researchers in [52] simulated the signal attenuation per meter in soil with varying parameters (i.e. sand, clay, water, the carrier frequency). In figure 4.4a, the volumetric water content of soil and carrier frequency remains constant in 5% and 2.4 GHz, and the sand and clay composition of soil varies. In this scenario, the signal attenuation varies from 10 dB to 90 dB for different compositions of sand, clay, and silt. Figure 4.4b presents signal attenuation per meter in varying carrier frequencies and volumetric water contents (0%-25%), and the mixture of soil is 50% sand, 15% clay, and 35% silt and remains constant. In this simulation, the signal attenuation per meter that varies from 40 dB to 140 dB (in 2.4 GHz carrier frequency and volumetric water contents from 0%-25%, respectively) is higher than the signal attenuation per meter for varying sand-clay composition in rather dry soil (i.e. with 5% volumetric water content). Hence, the effect of volumetric water content on signal attenuation is dominant compared to other parameters. We employ this fact to provide an estimation for the read range of wireless sensor module in the underground environment. To this aim, we do our experiments in a water environment that has specific properties and set an experiment shown in figure 4.5. The wireless sensor module is located in the water-resistant bag and submerged in water and so-called transceiver 1. The RSSI

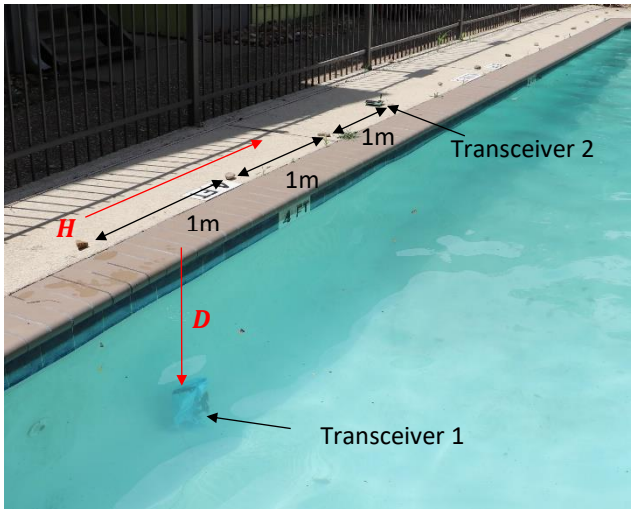

Figure 4.5. The strength of the radio signal at water medium. Transceiver 1 is located in a water resistant bag and submerged in a bucket of water. The depth of water is 1 m and the transceiver 2 is located on the ground a moves horizontally. D is the vertical distance of transceivers and H is the horizontal distance between receivers.

module is located aboveground and so-called transceiver 2. D is the distance of the transceiver 1 and transceiver 2 in which transceiver 1 is immersed in water (i.e. vertical distance), and H is the distance between two transceivers in the air (i.e. horizontal distance). We measured RSS for different values for D (i.e. 10 cm, 20 cm, 40 cm, and 100 cm) in which for each D, 16 measurements are done for different values for H ranging from 0 m to 15 m, and the results are shown in figure 4.6. In D =10 cm, RSS is -66 dBm and fluctuates around this amount with small changes in different values for H. In D = 20 cm, RSS is -73 dBm at $H \approx 0$ and fluctuates with small changes in different horizontal distances. At D = 40 cm, RSS is measured -80 dBm and does not change considerably at different horizontal distances. Also in D = 100 cm, RSS has measured -100 dBm and the changes in small in different horizontal values. We conclude from the results that the distance between two transceivers in the air does not affect the RSS. Also, the read range of the wireless sensor module in the water environment is around 1 meter. Hence, we have a wireless

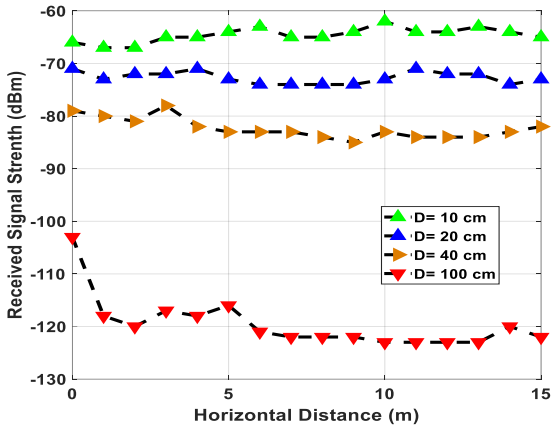

Figure 4.6. Received Signal Strength (RSS) at Different Horizontal (H) and Vertical Distances (D) of Transceiver 1 and Transceiver 2.

sensor module that penetrates the harsh environment and also can send the data packet of the five sensor measurements in 1 meter if only water (i.e. the most attenuating environment) is present with ≈ 0% packet error. In the real application that water is part of the environment, the read range is more than 1 meter. Our robot works in 9-in (0.23 m) to 22-in (0.56 m) diameter pipe and the rest of the environment is soil, so the read range is more than 1 meter. Based on the standards in [45], the pipelines are normally buried in 1.5 m beneath; considering the maximum allowable pipe diameter for our robot (i.e. 0.56 cm), the RSS is around -80 dBm and given -100 dBm for the correct realization of data packets, there is 20 dBm (i.e. 50 dB) path loss is allowable. The allowable path loss matches the results in figure 4.3a for path loss per meter in 2.4 GHz. The carrier frequency of our system is 434 MHz that experiences less path loss compared to the 2.4 GHz carrier frequency. Hence, we can say that our system can send the data packets to the aboveground surface from the underground environment for correct realization. The distance is sufficient for application and we will propose an operation procedure for the robot by this wireless sensor module that ensures a reliable communication link at this distance. However, since the wireless sensor module needs an antenna and we have limited space in the confined space of the central

processor, the embedded system needs to be designed to meet this requirement. In the next section, we design the embedded system and present the assembling in the robot.

4.3. System Implementation (Electrical and Mechanical)

The implementation of our robot consists of electrical design and mechanical assembling of the embedded system in the central processor. The electrical hardware of the system includes a power management circuit, analog drivers for the robot's actuators, analog sensors, and a low-power embedded system that controls the motion of the robot, acquires the sensors data, and provides a bidirectional data communication link with the base station.

4.3.1. Electrical System (PCB Design)

4.3.1.1. Power Management

A 12V lithium rechargeable battery with a capacity of 18A.h is the power source of the system. Regarding the analog and digital circuits as the main subcircuits of the electrical design, three DC voltage levels of 12V, 5V, and 3.3V need to be regulated and supplied. Therefore, while the battery voltage (VBAT) supplies the motor drives directly, it is stepped down to less than 6V through a high-efficiency DC-DC buck converter (TPS62150, Texas Instrument -TI-), and then is regulated to 5V and 3.3V through a dual-channel low-noise low drop-out linear voltage regulator (TPS7A87, TI). The two-step voltage regulation provides efficient power consumption and besides, minimizes the dissipation as heat. The 5V output voltage supplies analog sensors, the logic supply of the drivers, and the microcontroller. Also, the 3.3V provides the power for the RF transceiver (i.e. CC1200) and the IMU (i.e. BMI160). Current consumption corresponding to each of these three regulated DC voltages and the amount of noise each of the digital, analog, and RF subcircuits generate, directly affect the design of the PCB of the electrical system, the number of layers, and independent islands. Also, isolated ground planes for the loads connected to the 12V and for the sub-circuits supplied by 5V and 3.3V are considered, too.

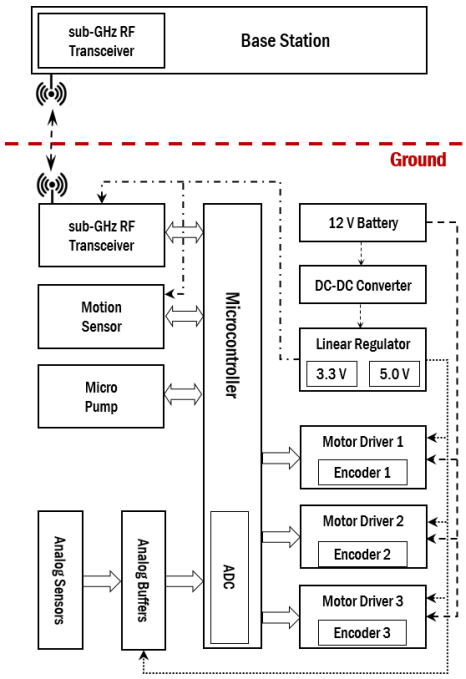

Figure 4.7. The Block Diagram the Printed Circuit Board (PCB) of the Robot.

4.3.1.2.Microprocessor and Digital Circuit

A low-power microcontroller (ATmega2560, Atmel) is the heart of the embedded system. It controls the robot drivers, establishes a serial peripheral interface (SPI) data communication with the CC1200, and communicates with the IMU (i.e. BMI160) through an inter-integrated circuit (I2C) protocol. Furthermore, the MCU has an embedded analog-to-digital converter (ADC) which takes samples from four analog sensors with 10 bits resolution. The RF transceiver implements a bidirectional data communication link with the stationary units through the MCU to transmit sensors' digitized samples and receive robot motion control commands. Due to incompatibility in the DC supply rating between the MCU (powered by 5 V) and the RF transceiver and the IMU (powered by 3.3 V), it was not possible to connect the SPI and I2C data buses between them. In this regard, the data lines are connected through digital buffer gates (SN74LVC2G34, TI). While

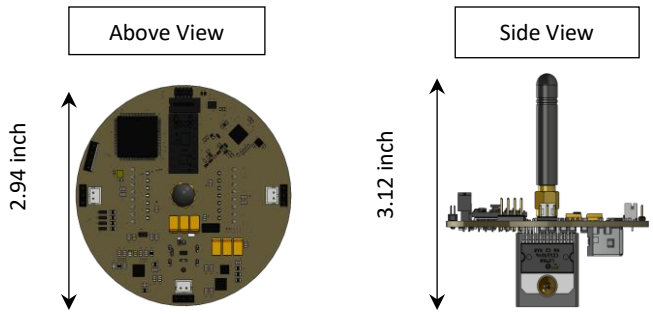

Figure 4.8. The Designed Printed Circuit Board (PCB).

the buffers accept an input voltage of 5V, the output is limited to the DC power supply of the buffers, which is 3.3 V.

4.3.1.3.The Robot Drivers and Analog Circuit

To drive the three wings of our robot, two high-current full-bridge dual drivers (L298, STMicroelectronics) provide the electrical control for the motors. Control input lines to the drivers are controlled through a pulse-width modulation (PWM) provided by the MCU and hence, motors can be driven independently and simultaneously. Besides, each motor is equipped with an encoder that measures the angular velocity of the motors as discussed earlier in this paper. Also, the system is equipped with a piezoelectric diaphragm micropump (mp6, Bartels Mikrotechnik) for pumping liquids inside our robot with varying flow rates controlled by a controller (mp6-OEM). In the design, we adopted for our application, frequency, and amplitude to the micropump are predefined by the internal circuit [97]. Furthermore, five analog sensors are added to the system to multi-parameter measurements for water quality monitoring. The Four sensors provide the output in terms of change voltage and the nature of the fifth one's output is current (i.e. miniaturized sensor for chlorine measurement in water [58]). In this regard, five analog buffers between the sensor's outputs and the ADC inputs of the microcontroller based on low-power operational amplifiers (OPA191, TI) are designed. Since the output values of four voltage-output sensors vary in the range of -0.5V to 0.5V, the analog buffers are designed such that the ADCs read values centered at half

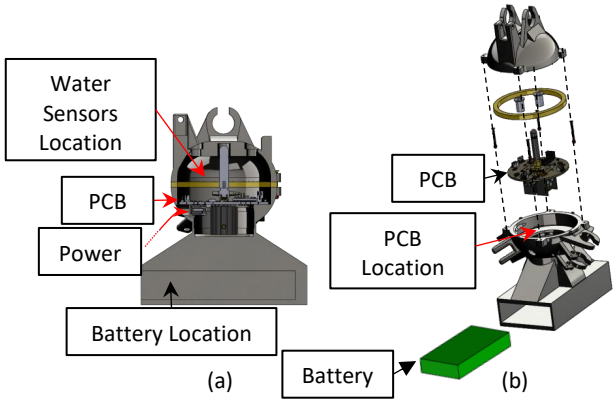

Figure 4.9. Location of the Printed Circuit Board (PCB) in the Central Processor. a) Cross-section View. b) Exploded View.

of their reference voltage. The voltage-output sensors values are mapped to 1.25+0.75V_{sensor} through a voltage divider and then, sampled by the ADCs. Therefore, V_{sensor} should be extracted through (V_{ADC}-1.25)/0.75. The output of single current-output sensor varies in the range of 0 to 50 A and so, needs to be converted to voltage through passing an appropriate resistor. The PCB antenna is a terminal antenna with a surface mount assembly (SMA) connection. It is designed for a frequency range of 433.05 434.79MHz and 0 dBi gain from Taoglas Inc. [98]. In figure 4.7, the hardware architecture of the PCB and the connection of different components are shown.

4.4. Mechanical System

Figure 4.8 shows the designed PCB for our robot. It is located in the central processor (see figure 4.9) in which the diameter of the PCB is 2.94 in and is placed on the surface in the control part. A hole is designed on the central processor to make enough space for the motor drivers and facilitates faster heat transfer. Power from the battery is connected to the PCB by a wire through a sealed hole on the central processor.

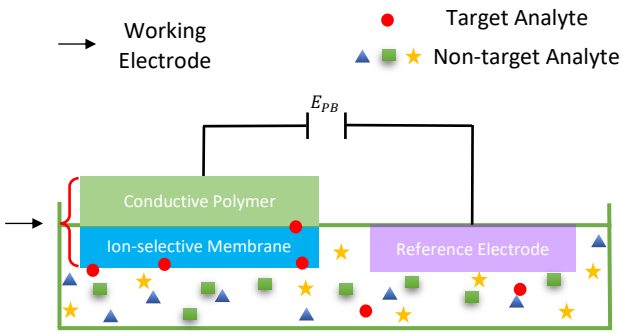

Figure 4.10. Operation Principle of miniaturized water sensors. The ion-selective membrane absorbs the target analyte and produces a voltage (E_{PB}) with respect to the reference electrode that is silver-silver chloride (AgCl). Source: Adapted from [98].

4.4.1. Ion-selective Water Sensors

The proposed robotic system is primarily designed for continuous water quality monitoring in WDS. There are various parameters in water that need to be monitored and different water sensors are designed to this aim. However, since there is space limitation in pipe, it is needed to have miniaturized sensors to locate them in the limited space of the central processor. Researchers have recently developed kind of miniaturized sensors that are suitable for small-sized environments (e.g. inside pipes) and work based on ion selection principle. In these sensors, two electrodes (working and reference electrodes) produce a potentiometric voltage based on the concentration of the ion (target analyte). For example, PH is an important parameter of potable water that is needed to be

Table 4.4. Specifications of water sensors in the smartcrawler.

Measuring Parameter	Associated Ion (Target Analyte)
PH	H^+
Chloride	Cl^-
Nitrate	NO_3^-
Calcium	Ca^{2+}
Sodium	Na^+

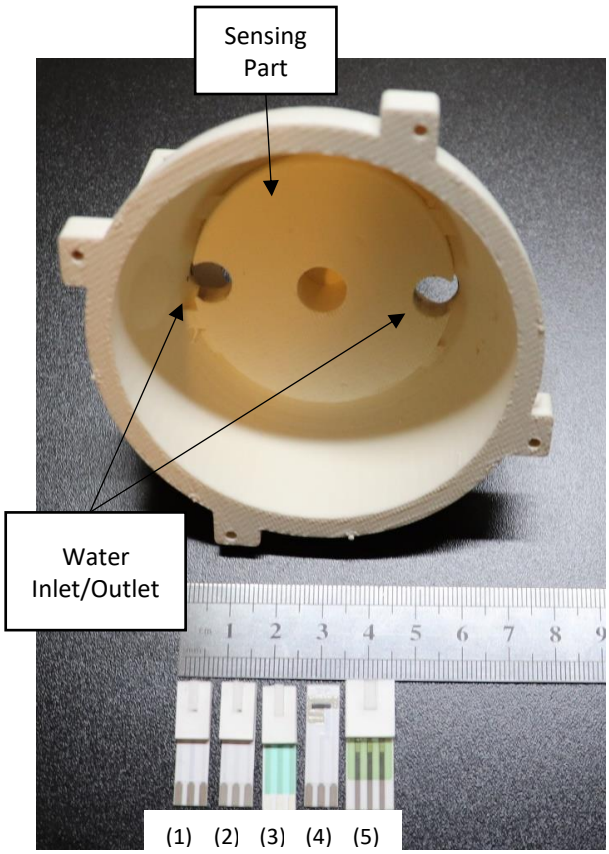

Figure 4.11. The commercial-off-the-shelf (COST) water sensors and their dimension compared to the sensing part. (1) PH Sensor. (2) Chloride Sensor. (3) Nitrate Sensor. (4) Calcium Sensor. (5) Sodium Sensor.

a specific range (6.5-9.5 [99]) in potable water and hydrogen ions, H^+ is associated with this parameter. Hence, PH of a solution can be measured by measuring the concentration of H^+ in that solution. Figure 4.10 shows the operation principle of an ion-selective sensor. The working electrode includes an ion-selective membrane and a conductive polymer that pass the target analyte and the reference electrode is mainly manufactured by silver-silver chloride (Ag/AgCl) and the relative voltage (E_{PB}) is measured between the electrodes. The electrodes are printed on a substrate and are located at a distance and there is a sensing area in which the solution is placed. The value of the parameter (e.g. PH) can be computed by E_{PB} using the Nernst equation [100]. Different

parameters can be measured with the ion-selection principle [99] and considering the size of the sensors, multi-parameter measurements are facilitated that is desirable. Figure 4.11 shows five miniaturized sensors (Table 4.4) from Zimmer and Peacock Corporation that can be embedded into the sensing part of the central processor. The dynamic range of the sensors is similar to the sensors we used for proof of concept of the proposed wireless sensor module. Since the sensors work based on an electrochemical process, they have rather long response of around one minute. In other words, once the sensor received water samples, it needs around one minute to have a settled output that requires the robot to stop at one location with stabilized configuration for a while. The multi-phase motion controller facilitates this requirement for the robot. In our design, the micro-pump system provides water samples through water inlets and outlets in the central processor for these sensors. The working and reference electrodes in each sensor have a pad that facilitates external connection to the data acquisition unit via wire. Also, these chemical sensors have a limited lifetime and need to be replaced and the module design of the robot facilitates easy replacement of the sensors.

We designed an integrated robotic system that can perform multi-parameter measurements with ion-selective sensors for water quality monitoring in different locations of WDS.

4.5. Notes and References

The conventional wireless sensor modules that are used for terrestrial applications (e.g. Bluetooth and ZigBee) are not practical for wireless underground applications because of highly attenuating environments of soil, water, and rock [52], [90], [93], [101]–[105]. We designed a bi-directional wireless sensor module that can penetrate the underground environment. We also measured its read range with experimental results and also the path loss of the soil and rock that is explained in [52] in which it can send data packets wirelessly from the underground environment to the aboveground surface with 1.5 m burial depth of pipes [45]. The researchers in [106], [107] investigates the reliability of wireless communication link between the underground and aboveground environment with numerical analysis and RSS. However, we developed and validated our wireless system to be suitable for data transmission with high data throughput for multi-parameter measurement with miniaturized water quality monitoring sensors that work based on the ion-selection technique.

5. OPERATION PROCEDURE FOR THE ROBOT[*]

5.1. Introduction

So far, an integrated robotic system that is equipped with a wireless sensor module and multi-phase motion controller is designed. It is desired that the robot have long-travel inspection with smart navigation. Hence, it is needed to localize the robots inside networks and also facilitate smart navigation. The researchers use different methods for localization of untethered in-pipe robots that are based on numerical and wireless radio frequency methods. The methods based on the numerical techniques rely on the information from the using ultrasonic sensors [108], camera [109], or laser rangefinder [110] sensors. The information from these sensors is used with the recent numerical methods (e.g. Kalman filter and Particle filter) to estimate the location of the in-pipe robot. In [62], the authors use a hydrophone and the RaoBlackwellised particle filter (RBPF) to localize the robot in pipeline and also create the map of pipeline at the same time (simultaneous localization and mapping (SLAM)). The non-straight configurations of the pipelines (e.g. bends or Tees) can be used for localization as landmarks. Using a vision-based landmark detection technique, the authors in [111] developed a pattern-matching image-processor method to recognize the shadow of elbows and branches in pipelines. However, the drawbacks of the systems without wireless systems are twofold: it is not possible to transceive data between the robot underground and the base station above ground during operation. Also, since there is no connection to the robot during operation, if failure (of motion) occurs during operation, it is not possible to localize the stuck robot in the pipeline. Hence, these methods limit the traveling distance of the in-pipe robots.

[*]Reprinted with permission from A Localization and Navigation Method for an In-Pipe Robot in Water Distribution System Through Wireless Control Towards Long-Distance Inspection" by Saber Kazeminasab, M. Katherine Banks. 2021. IEEE Access, pp. 117496-117511, Copyright 2021 by IEEE.

RSS is usually used for localizing the robot in the methods using wireless radio signals. In [107], the authors present the idea of relay nodes that are placed on the ground and are used for communication and localization of the robot, and optimized the number of the relay nodes in straight path that is needed to localize an in-pipe robot in [106], and present a localization method based on RSS from the in-pipe robot by dividing the long straight pipe to low-confidence and high-confidence zones in [57]. However, this method (that is limited to the straight path) does not consider non-straight conjurations of water network. Also, the authors in [112], [113] use extreme-low-frequency electromagnetic pulse (ELF-EP) that can penetrate metal pipes and also moving sensor array above ground for localization of in-pipe robot. The robots need to have smart navigation as well in pipelines.

In chapter 4, we proposed a bi-directional wireless sensor module that can send the data packets wirelessly from the underground pipelines to the aboveground surface. Using this wireless sensor module, in this chapter, we propose a localization method to localize the robot in complicated configurations of pipelines. In addition, we develop a navigation method to enable the robot to move in complicated configurations of pipeline and propose an operation procedure for the robot that facilitates regular measurements of parameter(s) in water in the long-distance inspection.

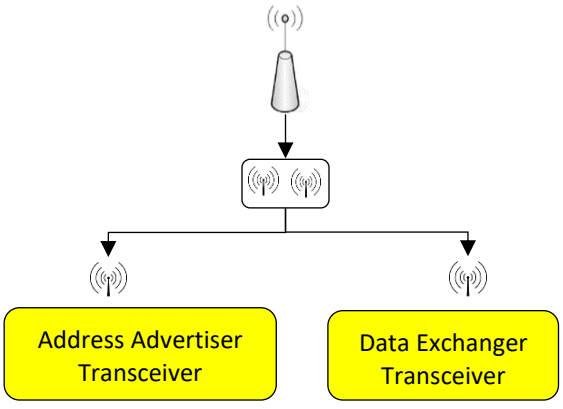

Figure 5.1. Each relay node (RN) comprises two parts: Address Advertiser Transceiver (AAT) and data exchange transceiver (DET).

5.2. System Hardware

Our proposed wireless robotic network includes:

- One wireless sensor module is mounted on the in-pipe robot and moves with it during operation.
- Some fixed relay nodes (RN) above ground.

The wireless sensor module on the robot synchronizes the wireless sensor, micro-pump system, and the motion control units and we explained it earlier in this paper. We call the transceiver on the robot, moving transceiver (MT) for brevity. The RNs include two radio transceivers that are connected to the host MCU. One transceiver always advertises an address signal on air and the other one exchanges data with the robot. We call the transceiver that advertises the signal, address advertiser transceiver (AAT), and the transceiver that exchanges data, data exchange transceiver (DET) (see figure 5.1). The RNs are located at special configurations of the pipeline like bend, wyes, and T-junction. Figure 5.2 shows the overall view of the proposed wireless robotic sensor

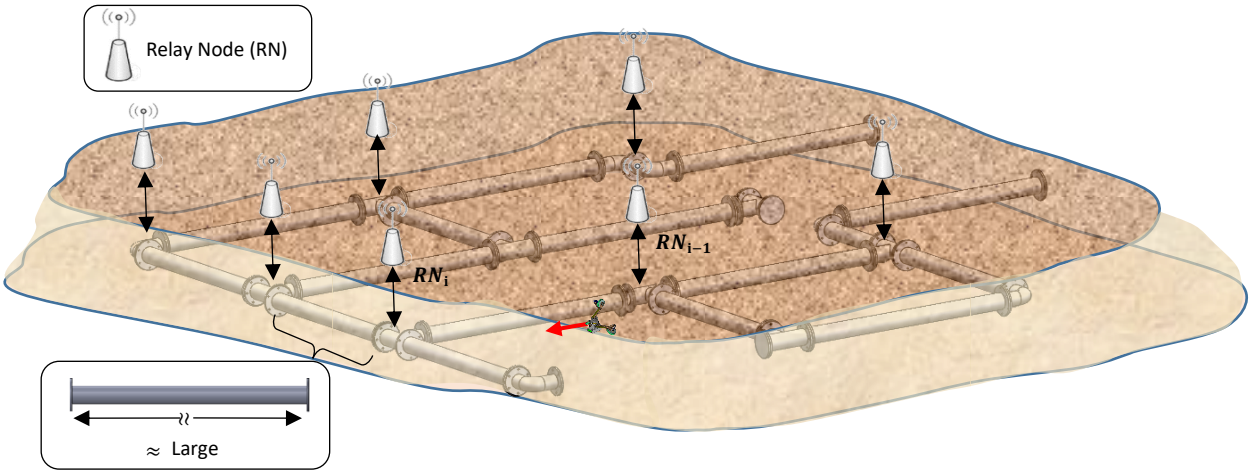

Figure 5.2. Overall View of Our Proposed Robotic Network. The robot moves inside pipe underground and the RNs are located at special configurations of the pipelines like bends and T-junctions. The distance between the RNs is large.

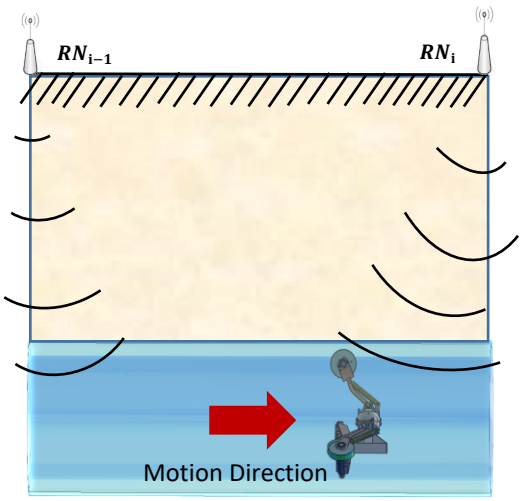

Figure 5.3. Part (1) of the Proposed Operation Procedure: The robot moves from RN_{i-1} to RN_i and the robot does not have wireless communication with relay nodes.

that the robot moves inside the pipeline underground and the RNs are located at special configurations of the pipeline above ground.

5.3. Operation Procedure

The operation procedure of the robot divides into five parts:

(1) Motion in Straight Path with No Wireless Communication: The robot moves in straight path between two consecutive RNs (RN_{i-1} to RN_i). The robot does not have wireless communication (see figure 5.3).

(2) Establishing Communication between the Robot and RN_i: The robot establishes wireless communication with RN_i once it reaches the read range of RN_i.

(3) Sensor Measurement, Processing, and Wireless Transmission from the Robot to the RN_i: The robot starts sensor measurements, processes them, and transmits the processed sensors measurements to the RN_i.

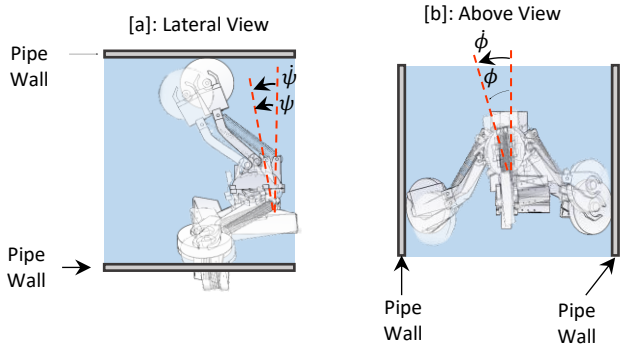

Figure 5.4. Stabilizing States of the Robot.

(4) Wireless Transmission from the RN_i to the Robot: The RN_i transmits the motion control command to the robot.

(5) Change of Direction of the Robot: After the robot received the motion command signal, it changes its direction and starts moving in a straight path until it reaches the radio range of the RN_{i+1}.

The operation procedure of the robot is in a way that the robot switches between different control algorithm modes and data transmission directions. In following, we explain each part of the procedure in detail.

5.3.1. Part (1): Motion in a Straight Path with No Wireless communication

In this phase of the operation, the robot moves in straight path and does not have wireless communication with RNs. The motion controller in this phase stabilizes the robot and enables it to track a constant velocity. To have a measure of stabilization for the robot, we define rotation

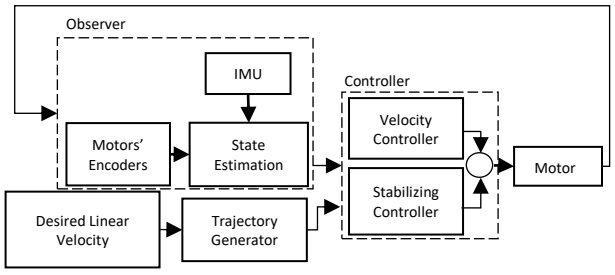

Figure 5.5. The controller to stabilize the robot and track the desired velocity in straight paths.

around the y-axis (ϕ), z-axis (ψ), and their derivatives, $\dot{\phi}$ and $\dot{\psi}$ (see figure. 5.4). The controller effort for the stabilization task is to keep the stabilizing states of the robot, $[\phi \quad \psi \quad \dot{\phi} \quad \dot{\psi}]$ at zero [75], [114]. To this aim, we designed a controller that is the linear quadratic regulator (LQR) and stabilizes the robot. Also, the robot needs to track a desired velocity during operation. Another controller is proposed which is based on a PID controller to this aim. If all the three wheels of the robot have equal angular velocity, the linear velocity of the robot is calculated based on one wheel's angular velocity. So, to have a defined linear velocity, we proposed three PID controllers to control the velocity of each wheel. The LQR and PID controllers are combined to fulfill both requirements in a straight path. Figure 5.5 shows the controller algorithm diagram in this phase. The observer in the controller algorithm fuses the data from an inertial measurement unit (IMU) which is placed in the central processor and three encoders at the end of the wheels. The encoders measure the angular velocity of the wheels. Hence with this architecture, we have a sense of orientation of the robot and odometry for it. We validated the performance of the controller in this phase with experimental results in chapter 3.

5.3.2. Part (2): Establishing Communication between the Robot and RN_i

The robot moves in a straight path inside the pipe (underground) from RN_{i-1} toward RN_i. On the ground in RN_i, one transceiver on the RN_i is in transmit mode and advertises the RN_i's location order continuously. The location order is the address of the RN_i in the network that we call "relay node address" or RNA in short. For example, the RN_1 is the first relay node in the network in which the robot approaches to and the RNA for it (i.e. RN_1) is 1. The RN_2 is the second one in the network and its RNA (i.e. RN_2) is 2, and so on. Since each RN advertises a unique RNA, the possible overlap between radio signals of multiple RNs does not confuse the robot.

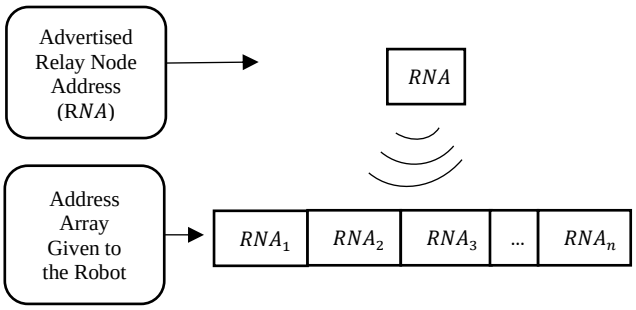

Figure 5.6. Advertised RNA and the address array that is programmed in the robot firmware.

On the robot side, the robot needs to distinguish the right RN in the network. This way it can switch to the right control algorithm that facilitates appropriate motion during operation. In other words, the robot needs the map of operation path. Our solution to give the robot a sense of the map of the pipeline is to put the RNs in the special configurations of the pipeline network and give the robot an array that contains the RNAs and their orders in the network:

$$\text{RNA} = [RNA_1 \quad RNA_2 \quad \ldots \quad RNA_n] \tag{5.1}$$

In (5.1), the RN_i reveals the information about the configuration type. The configuration type can be 90° bend, 45° bend, 135° bend, T-junction, etc. The robot is programmed in a way that knows the configuration shape associated with specific RNA. For example, the configuration associated with RN2 is a 90°-bend. Hence, the control algorithm chooses the control phase that steers the robot in a bend-shaped pipe. Figure 5.6 shows the advertised RNA and the array in the robot's firmware. Algorithm 1 defines the configuration type of the pipe where the robot is located. The *Interrupt_Service_Routine* (i.e. built-in function in MCUs) in the algorithm is triggered once RNA is received by the wireless sensor module on the robot. The *Interrupt_Service_Routine* sets a defined flag so-called *wireless_flag* that triggers the process of defining the configuration type. First, the *wireless_flag* is unset for the next interrupt of the wireless sensor module, then a variable, CT, is defined to store the value of configuration type, and finally, two variables, done and i are

Algorithm 1: Pipe Configuration Type Determination Steps in Phase 2 of the Operation Procedure.

```
If (wireless_flag) {
        wireless_flag=0;
        CT=0;  CT::Configuration Type
        done = 0;
        i=1;
        while (!done){
        | If (RNA_i == RNA){
        | |  CT=  RNA_i
        | |  done=1;}
        | else
        | |{i = i + 1};
        | end
        }
    Interrupt_Service_Routine{
    wireless_flag=1;
    }
```

defined that stops the searching process and counts for the elements in **RNA** matrix, respectively. In the searching process, RNA is compared to the elements of **RNA** matrix; if i^{th} element matched RNA, RNA_i is stored in CT and the searching process stops by setting done. The motion controller [9]. The motion controller in this part of the procedure is a stabilizer controller and we evaluated the performance of the controller in chapter 3. Hence, we localize the robot in the network with the wireless sensor module and the non-straight configurations of water network.

5.3.3. Part (3): Sensor Measurement, Processing, and Wireless Transmission from the Robot to the RN_i

So far, the robot has received an RNA, stopped moving, and is localized. The micro-pump system at this time activates and provides water samples for the onboard water quality monitoring sensors (we explained their operation principle in chapter 4). To activate the micro-pump, a pin on the micro-pump driver is set and the driver activates the micro-pump with the constant flow rate of 7 ml/min. that are designed and developed by our team [58]. These chemical sensors operate based on chemical reactions and their output converges to a specific value after around one minute [58]. The firmware remains idle for one minute and no function is implemented during this time and also the robot stays in the stabilized configuration with zero velocity until the output of the sensors settles. The sensors are connected to the host MCU. After their output is settled, the analog

Algorithm 2: Phase 3 of the Operation for Sensors Measurement, Processing, and Transmission.

1. Micro-pump Activation.
2. Idle State for One Minute (Sensors' Output Settlement)
3. ADC Activation (Start Sensor Measurement).
4. Sensor Measurement Processing.
5. Data Packet Creation (Compatible with Communication Protocol).
6. Update the MT's Payload with Data Packet.
7. RX Mode ⟶ TX Mode.
8. Data Packets Transmission.
9. Done Transmission (DT) Variable.
10. TX Mode ⟶ RX Mode.

to digital conversion (ADC) unit of the MCU starts sensor measurements. The MCU then processes raw sensor data to compute the real value of the target analyte. The processing includes filtering noisy data, converting current to voltage, and applying the associated chemical formula to calculate the real value for the target analyte. Then a data packet that is compatible with the communication protocol is created that is an array that includes the preamble bytes, packet length, the packet counter, and processed sensor data. The payload of the MT is then updated with the data packet. The MCU at this state goes to transmit mode and transmits the packet to the RN_i. The transceiver on the RN_i (that is in receive mode) receives the packet. After the MCU transmits all data packets, it sends a separate data packet that includes a variable called Done Transmission (DT) to the RN_i, to acknowledge that the data packets are sent completely, and then MT goes to receive mode. Algorithm 2 shows the procedure in phase 3 that is related to the sensor measurement, processing, and transmission.

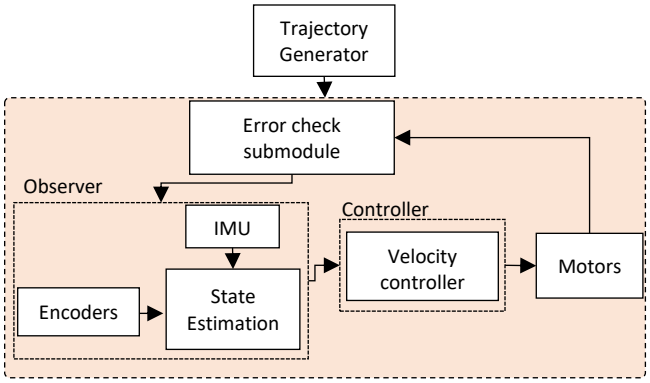

Figure 5.7. The Motion Control Algorithm for Non-straight Paths.

5.3.4. Part (4): Wireless Transmission from RN_i to the Robot

In this phase, the RN_i sends a motion control command to the MT. Based on the configuration type that is already defined in part 2 of the operation, the robot chooses the control phase designed for a non-straight configuration that steers the robot in the desired direction. Based on literature, non-straight configurations are challenge for in-pipe robots to pass through and require appropriate motion controller [16], [38], [41], [47], [50], [71], [82], [83], [115], [116]. We propose a new controller that facilitates rotation for the in-pipe robot based on the differential motion for the wheels. The controller includes a trajectory generator block, an observer block, an error-check sub-module, and a velocity controller based on three PID controllers. The trajectory generator creates differential motion in which different angular velocities for the wheels, change the direction of motion of the robot. The error-check submodule monitors the amount of rotation around the desired axis and allows the controller in the non-straight phase to continue until the defined amount of rotation is acquired. Figure 5.7 shows the control algorithm for the non-straight configuration. To evaluate the performance of this phase of the controller, we modeled the robot in AMDAS software which is a multibody dynamic simulator and implemented the controller in the MATLAB Simulink environment. Then we linked the control plant in MATLAB and the

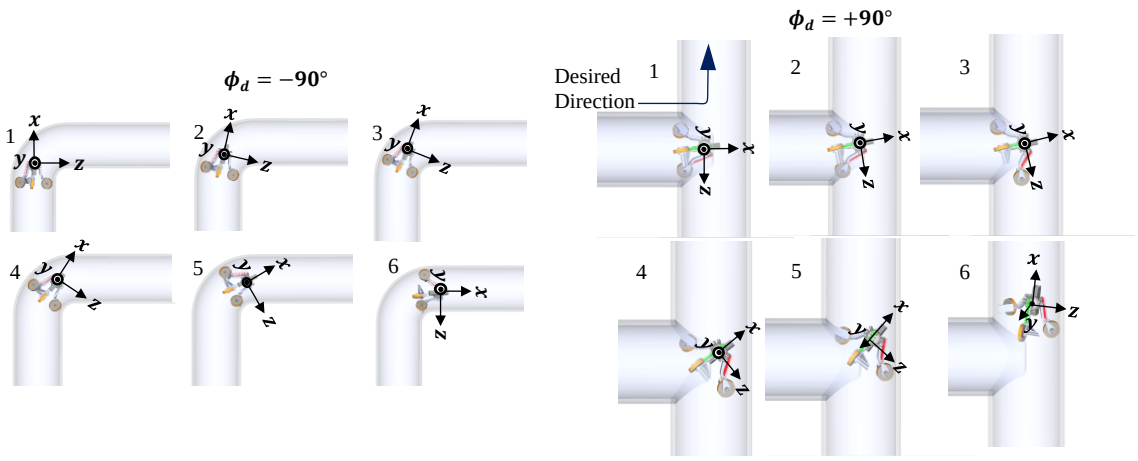

(a) (b)

Figure 5.8. DAMS-MATALB Co-simulation Results for (a) 90° Bend and (b) T-junction based on Non-straight Controller.

simulated system in ADAMS software and co-simulated the robot-controller. Figure 5.8 shows the motion sequences of the robot in bend and T-junction. The results in Figure 5.8 prove that the motion control phases for the robot in T-junctions and bends can facilitate smooth motion for the robot in bends and T-junctions. We repeated our simulations and validated the robot can cover bends with diameters range 9-in to 22-in and also T-junctions with diameters ranging from 9-in to around 15-in. Once the rotation is completed, the robot is located in a straight path and continues moving in a straight path. The control phase here is again the stabilizer-velocity tracking controller in figure 5.5.

5.3.5. Part (5): Change of Direction of the Robot

The robot switches to the non-straight controller phase and changes its direction to the desired direction. The robot communication with RN_i stops during rotation. Figure 5.9 shows switching between different motion control phases and communication direction modes during operation. We synchronized the wireless communication setup and the motion control algorithm in this work. Figure 5.10 shows the overall view of the synchronized wireless control for the operation

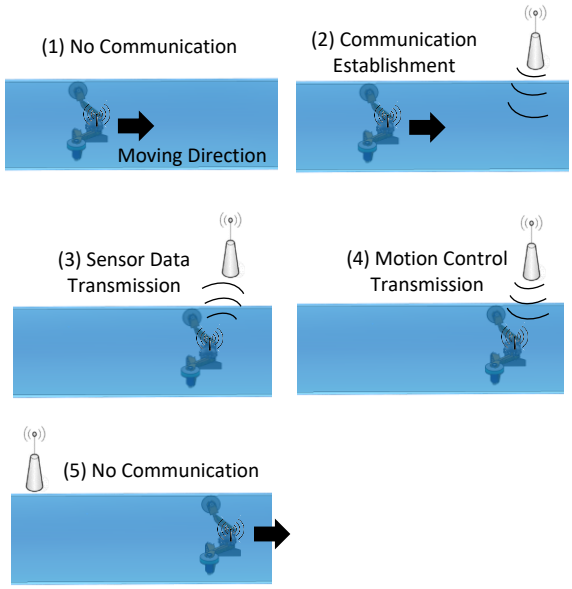

Figure 5.9. Wireless Communication Switching in the Proposed Operation Procedure for the Wireless Robotic Network.

procedure of the robot. Hence, the robot navigates between different configurations of the pipelines by synchronization of the wireless sensor module and the multi-phase motion control algorithm.

5.4. Experiment

In this part, we evaluate the performance of the developed operation procedure with experiment. To this aim, a relay node is configured with two CC1200 evaluation modules in 434 MHz that are connected to the two MCU Launchpads (see figure 5.11). The robot is located in a 14-in diameter pipe. Our goal is to investigate the functionality of the developed wireless control system. In other words, we validate if switching between phases of motion control occurs by the wireless. To this aim, the relay node sends a command to the robot and the robot starts motion with phase 1 of the controller (stabilizer-velocity tracking controller) and moves inside the pipe with 10 cm/s. The robot has the map of the operation as $\mathbf{RNA} = [1]$ as we have just one junction in our experiment. The relay node sends the $RNA = 1$ when the robot reaches the end of the pipe and it is expected that the robot stops at this location once it received the RNA. We performed the experiment and

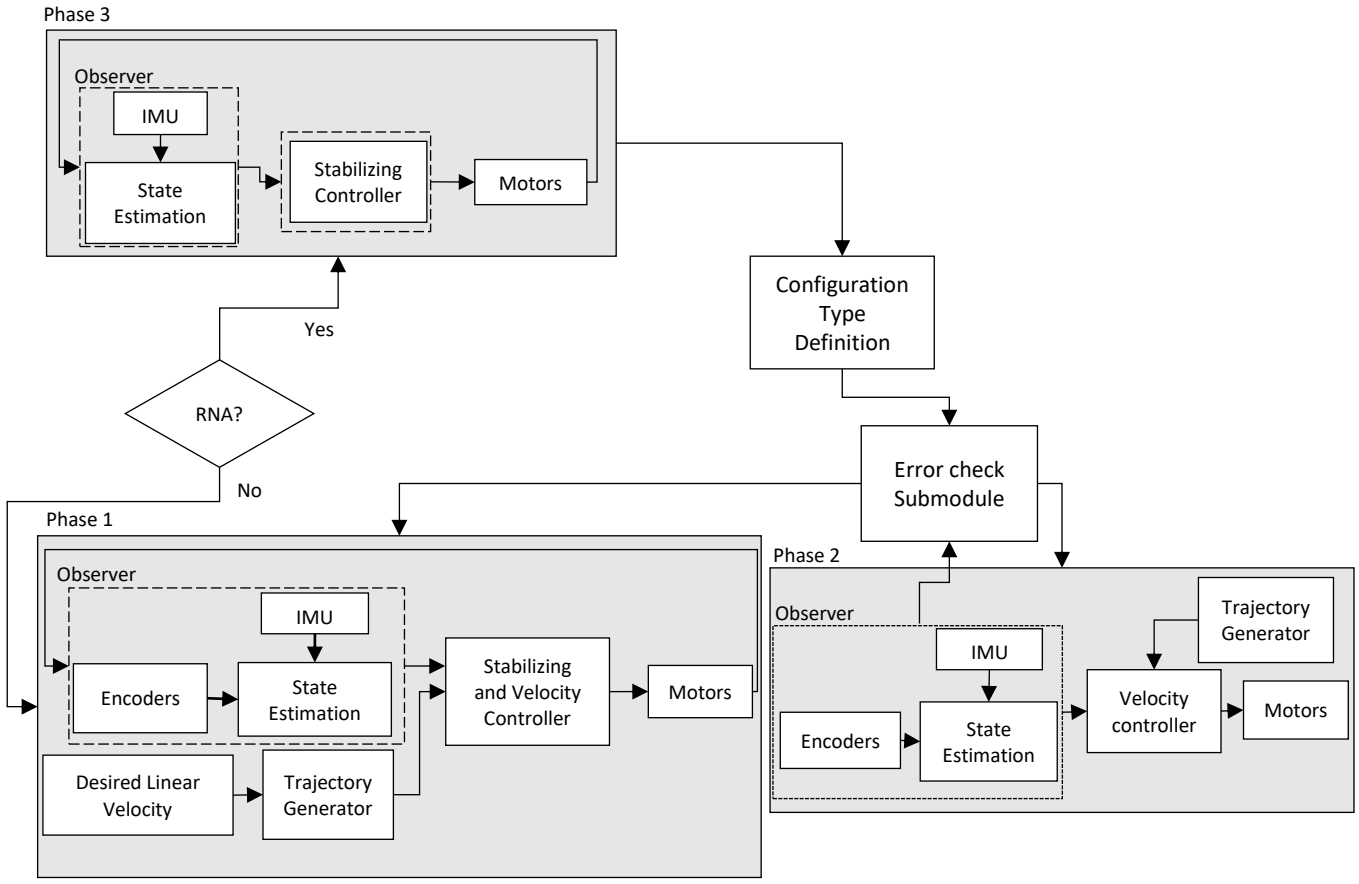

Figure 5.10. Synchronized Wireless Communication System with the Multi-phase Motion Control Algorithm. Switching between different phases of the motion control algorithm is performed with wireless system.

the results are shown in figure 5.12 in which the sequences of motion are shown from 1 to 4. The robot first stabilizes itself at the beginning of the motion and reaches the desired velocity (i.e. 10 cm/s) and moves with stabilized motion in the pipe. At the end of the motion, the relay node sent the $RNA = 1$ and upon transmission, the robot stopped there with the stabilized configuration. Hence, the robot switched from phase 1 to phase 2 of the motion controller and the developed wireless control is verified. In our experiments, we found out that the time at which the AAT sends the RNA is extremely important as the robot stops with the stabilized configuration once it receives

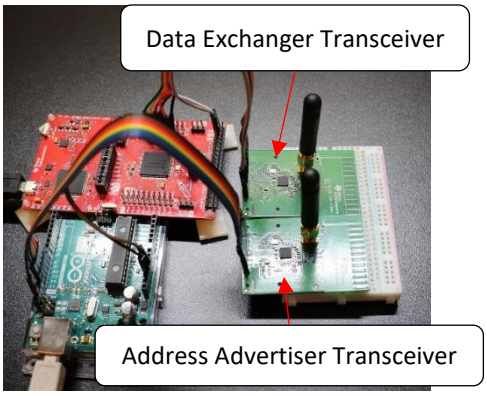

Figure 5.11. A Setup for One Relay Node. Each relay node (RN) comprises two parts: Address Advertiser Transceiver (AAT) and data exchange transceiver (DET). Two CC1200 evaluation modules are connected to two MCU Launchpads.

the RNA. In other words, the robot switches to another phase of the motion control algorithm. In some experiments, the robot stopped near the end of the pipe (desired location) while in other experiments, the robot stopped at other undesired locations. This is because the radio signal propagates spatially in the air and the robot may receive it at any location. This phenomenon is higher in our experiment than in water medium in which water medium limits the read range of the radio signal is not present and in real applications, this effect is less than in our experiment but still exists. We can address the issue by locating a rangefinder sensor in front of the robot and find the distance from the front obstacle and reach close enough to the junction with the stabilized motion (phase 1) in a straight path before switching to phase 2 of the motion controller.

5.4.1. Discussion on the Experiments

The developed operation procedure facilitates localization and navigation in complicated configurations of pipelines for the in-pipe robots that was a challenge in this field. Also, the proposed method facilitates long-distance inspection for the robot; since the distance between the relay nodes is large. The resilient of the robot that is coined and discussed in [72] is considered in this robot in which the spring mechanism that provides friction force between the pipe wall and

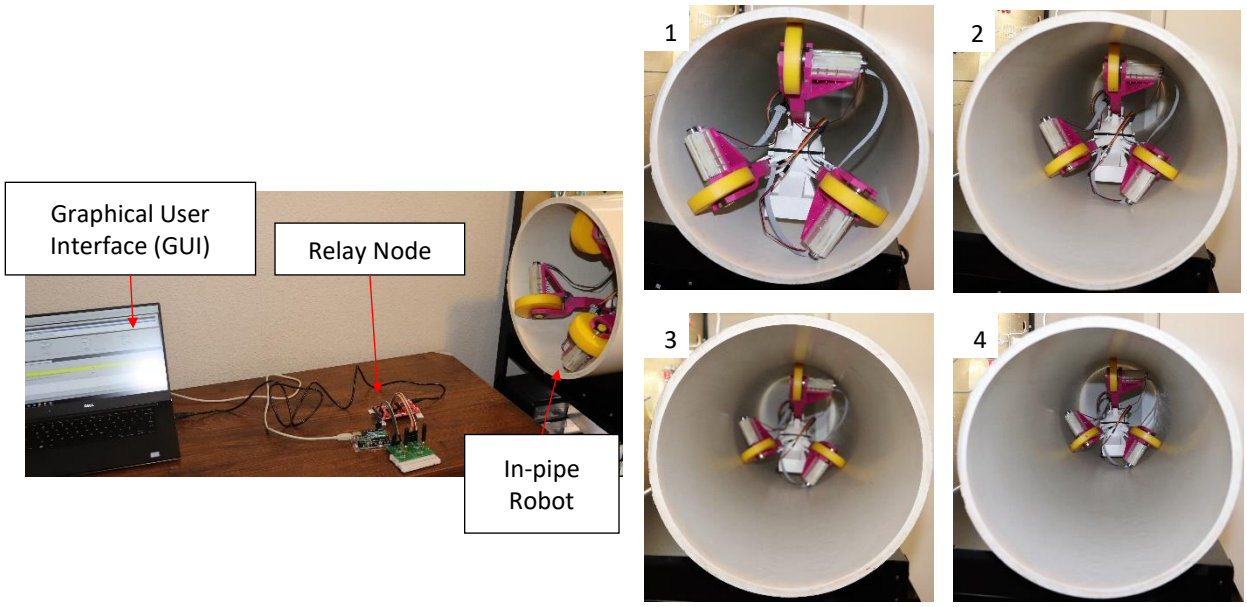

(a) (b)

Figure 5.12. (a) Experiment Setup: The in-pipe robot is located in a 14-in diameter PVC pipe. The relay node is connected to PC and the sends the $RNA = 1$ once the robot received at the end of the pipe. (b) Sequence of motion of the robot. The robot starts moving in (1) with phase 1 of the motion controller (stabilizer-velocity tracking controller) and reach to 10 cm/s velocity. Once the robot arrived at the end of the pipe, the relay node sends $RNA = 1$ and the robot stops with stabilized configuration.

the wheels is characterized based on the extreme operating condition in in-service networks as well as the battery capacity of the robot. The spring mechanism prevents the robot from collapse during operation and the characterized battery ensures enough operation duration that is at least 3 hours in the conditions the robot moves with 50 cm/s against the water flow with 70 cm/s [75]. Even in case, the robot fails during operation, it is easy to pinpoint the location of the failed robot with this method. We also validated the operation procedure in each step separately by experiment and simulations; the performance of the motion controllers are validated with experiments in straight path and simulation in non-straight configurations, the reliability of the wireless communication system is validated to ensure it can penetrate harsh environments of water and pipe, bi- directionality, and fast discovery between the robot and the relay nodes. The sensors that

measure the parameters of water have a rather long response time (around one minute [58]) and we considered their response time in the procedure. The developed procedure enables data transmission during operation which is useful in quality monitoring in long inspections. We also experimented with the wireless control to see its functionality to enable the robot for reliable motion in complicated configurations.

5.5. Notes and References

The operation procedure we proposed and validated in this chapter provides localization, navigation, and also data transmission during operation for the robot in complicated configurations of pipeline systems by synchronizing the multi-phase motion controller and wireless sensor module. Switching between different modes of closed-loop motion controllers is done with a wireless sensor module that facilitates smart navigation for the robot that is advantageous over [30], [49]. The map of the operation that is an array of non-straight junctions is programmed to the robot firmware. The spring mechanism and power supply of the system are characterized to have fully automotive motion against uncertainties and disturbances in the pressurized in-service pipeline network and also enough operation duration compared to [71]. The operation procedure using relay nodes in our method enables non-straight configuration navigation as well compared to [57]. It also takes the long response time of the chemical water quality monitoring sensors into account [58] by entering the robot to phase 3 of the motion controller that facilitates stabilized configuration with zero velocity. The proposed procedure using the idea of relay nodes, enables the users to pinpoint the failed robot if it collapses during operation that is advantageous over the systems using the information from the surrounding environment [64], [70], [109], [117]–[123].

6. CONCLUSION

In this research, we designed and prototyped an integrated size-adaptable in-pipe robotic system based on the under-actuated system and wheeled wall press mechanism that is waterproof and can operate in potable water distribution systems. The self-powered robotic system is characterized based on the real operation conditions to be fully automotive while the distribution system remains in service. We designed a multi-phase motion controller that stabilizes the robot and controls the velocity of the robot in straight paths and enables it to rotate around the two axes with the desired amount in non-straight paths. The stabilizer-velocity controller is based on a linear quadratic regulator (LQR) and proportional-integral-derivative (PID) controller and the controller for non-straight path works based on a trajectory generator block, error check submodule, and PID-based velocity controller to acquire differential motion. We also facilitated wireless underground communication with a bi-directional wireless sensor module that works based on active radio frequency identification (RFID). Our proposed wireless system enables a reliable and bi-directional communication link between the underground robot and the base station aboveground (i.e. with the received signal strength (RSS)> -100 dBm) in the highly attenuate environment of water, soil, and pipe for 1.5 m burial depth of pipeline networks with high data throughput. Based on the multi-phase motion controller and wireless sensor module, we developed an operating procedure that provides localization, smart navigation, and wireless data transmission for the robot during operation. To this aim, some relay nodes (RN) are located at non-straight configurations of the pipeline of the robot operation path. The RNs relay data between the robot and the central base station. The robot switches communication with different RNs during operation. Our robotic system can inspect long-distance inspection with smart navigation without the need to shut down the distribution network.

REFERENCES

[1] "Drinking Water Distribution Systems | Six-Year Review of Drinking Water Standards | US EPA." https://www.epa.gov/dwsixyearreview/drinking-water-distribution-systems (accessed May 02, 2021).

[2] E. P. A. Us, "Environmental Protection Agency. National Primary Drinking Water Regulations: Stage 2 Disinfectants and Disinfection By-products (DBP rule)," Fed. Regist. Washington, DC, pp. 387–493, 2006.

[3] P. Juuti, H. Mattila, R. Rajala, K. Schwartz, and C. Staddon, Resilient Water Services and Systems:: The Foundation of Well-Being. IWA Publishing, 2019.

[4] A. Selvakumar, J. C. Matthews, W. Condit, and R. Sterling, "Innovative research program on the renewal of aging water infrastructure systems," J. Water Supply Res. Technol., vol. 64, no. 2, pp. 117–129, 2015.

[5] A. Selvakumar and A. N. Tafuri, "Rehabilitation of aging water infrastructure systems: key challenges and issues," J. Infrastruct. Syst., vol. 18, no. 3, pp. 202–209, 2012.

[6] M. V Storey, B. der Gaag, and B. P. Burns, "Advances in on-line drinking water quality monitoring and early warning systems," Water Res., vol. 45, no. 2, pp. 741–747, 2011.

[7] B. D. Hohman, "Challenge studies of the pittsburgh distribution network pilot contamination warning system," University of Pittsburgh, 2009.

[8] N. Sankary and A. Ostfeld, "Inline mobile sensors for contaminant early warning enhancement in water distribution systems," J. Water Resour. Plan. Manag., vol. 143, no. 2, p. 4016073, 2017.

[9] D. M. Chatzigeorgiou, K. Youcef-Toumi, A. E. Khalifa, and R. Ben-Mansour, "Analysis and design of an in-pipe system for water leak detection," in ASME 2011 International Design

Engineering Technical Conferences and Computers and Information in Engineering Conference, 2011, pp. 1007–1016.

[10] R. Fletcher and M. Chandrasekaran, “SmartBall: a new approach in pipeline leak detection,” in International Pipeline Conference, 2008, vol. 48586, pp. 117–133.

[11] T. T.-T. Lai, W.-J. Chen, Y.-H. T. Chen, P. Huang, and H.-H. Chu, “Mapping hidden water pipelines using a mobile sensor droplet,” ACM Trans. Sens. Networks, vol. 9, no. 2, pp. 1–33, 2013.

[12] “PipeDiver® - Condition Assessment - Pure Technologies - Pure Technologies.” https://puretechltd.com/technology/pipediver-condition-assessment/ (accessed Nov. 03, 2020).

[13] L. Shao, Y. Wang, B. Guo, and X. Chen, “A review over state of the art of in-pipe robot,” in 2015 IEEE International Conference on Mechatronics and Automation (ICMA), 2015, pp. 2180–2185.

[14] L. Zhu and J. Chen, “A Review of Wheeled Mobile Robots [J],” Mach. Tool Hydraul., vol. 8, 2009.

[15] Q. LU, Y. ZHANG, L. SHEN, and J. QIAN, “Piping robots that suit the variation of pipe diameter [J],” J. Mach. Des., vol. 1, 2007.

[16] Y. Qu, P. Durdevic, and Z. Yang, “Smart-Spider: Autonomous Self-driven In-line Robot for Versatile Pipeline Inspection,” Ifac-papersonline, vol. 51, no. 8, pp. 251–256, 2018.

[17] H. R. Choi and S. M. Ryew, “Robotic system with active steering capability for internal inspection of urban gas pipelines,” Mechatronics, vol. 12, no. 5, pp. 713–736, 2002.

[18] D. Waleed et al., “An In-Pipe Leak Detection Robot With a Neural-Network-Based Leak Verification System,” IEEE Sens. J., vol. 19, no. 3, pp. 1153–1165, 2018.

[19] T. Ren, Y. Zhang, Y. Li, Y. Chen, and Q. Liu, “Driving Mechanisms, Motion, and Mechanics of Screw Drive In-Pipe Robots: A Review,” Appl. Sci., vol. 9, no. 12, p. 2514, 2019.

[20] J. Liu, X. Zhao, and M. TAN, “Legged robots: a review [J],” Robot, vol. 28, no. 1, pp. 81–88, 2006.

[21] K. Miyasaka, G. Kawano, and H. Tsukagoshi, “Long-mover: Flexible Tube In-pipe Inspection Robot for Long Distance and Complex Piping,” in 2018 IEEE/ASME International Conference on Advanced Intelligent Mechatronics (AIM), 2018, pp. 1075–1080.

[22] X. Jian, Y. Wang, and P. Yang, “Advances of bionic robot researches on earthworm peristaltic mechanism,” Chinese J. Constr. Mach., vol. 10, no. 3, pp. 359–363, 2012.

[23] H. Sato et al., “Proposal for Pipeline-Shape Measurement Method Based on Highly Accurate Pipeline Length Measurement by IMU Sensor Using Peristaltic Motion Characteristics,” in 2020 IEEE/ASME International Conference on Advanced Intelligent Mechatronics (AIM), 2020, pp. 874–881.

[24] P. Liljebäck, K. Y. Pettersen, Ø. Stavdahl, and J. T. Gravdahl, “A review on modelling, implementation, and control of snake robots,” Rob. Auton. Syst., vol. 60, no. 1, pp. 29–40, 2012.

[25] M. Kamata, S. Yamazaki, Y. Tanise, Y. Yamada, and T. Nakamura, “Morphological change in peristaltic crawling motion of a narrow pipe inspection robot inspired by earthworms locomotion,” Adv. Robot., vol. 32, no. 7, pp. 386–397, 2018.

[26] G. H. Mills, J. H. W. Liu, B. Y. Kaddouh, A. E. Jackson, and R. C. Richardson, “Miniature Magnetic Robots For In-Pipe Locomotion,” in Robotics Transforming the Future: Proceedings of CLAWAR 2018: The 21st International Conference on Climbing and Walking Robots and the Support Technologies for Mobile Machines, 2018, pp. 289–300.

[27] R. Kashyap, R. Kashyap, R. Kumbhar, and A. Chari, “Design of Reconfigurable In-pipe Exploration Robots,” in 2018 International Conference on Current Trends towards Converging Technologies (ICCTCT), 2018, pp. 1–6.

[28] M. Abdellatif, H. Mohamed, M. Hesham, A. Abdelmoneim, A. Kamal, and A. Khaled, “Mechatronics design of an autonomous pipe-inspection robot,” in MATEC Web of Conferences, 2018, vol. 153, p. 2002.

[29] Q. Liu, T. Ren, and Y. Chen, “Characteristic analysis of a novel in-pipe driving robot,” Mechatronics, vol. 23, no. 4, pp. 419–428, 2013.

[30] Y.-S. Kwon and B.-J. Yi, “Design and motion planning of a two-module collaborative indoor pipeline inspection robot,” IEEE Trans. Robot., vol. 28, no. 3, pp. 681–696, 2012.

[31] D. Lee, J. Park, D. Hyun, G. Yook, and H. Yang, “Novel mechanisms and simple locomotion strategies for an in-pipe robot that can inspect various pipe types,” Mech. Mach. Theory, vol. 56, pp. 52–68, 2012.

[32] P. Li, S. Ma, B. Li, Y. Wang, and Y. Liu, “Self-rescue mechanism for screw drive in-pipe robots,” in 2010 IEEE/RSJ International Conference on Intelligent Robots and Systems, 2010, pp. 2843–2849.

[33] J. Nagase and F. Fukunaga, “Development of a novel crawler mechanism for pipe inspection,” in IECON 2016-42nd Annual Conference of the IEEE Industrial Electronics Society, 2016, pp. 5873–5878.

[34] R. Tao, Y. Chen, and L. Qingyou, “A helical drive in-pipe robot based on compound planetary gearing,” Adv. Robot., vol. 28, no. 17, pp. 1165–1175, 2014.

[35] E. Dertien, M. M. Foumashi, K. Pulles, and S. Stramigioli, “Design of a robot for in-pipe inspection using omnidirectional wheels and active stabilization,” in 2014 IEEE International Conference on Robotics and Automation (ICRA), 2014, pp. 5121–5126.

[36] Y.-S. Kwon and B.-J. Yi, “Development of a pipeline inspection robot system with diameter of 40mm to 70mm (Tbot-40),” in 2010 IEEE International Conference on Mechatronics and Automation, 2010, pp. 258–263.

[37] S. Jerban and M. M Moghaddam, “On the in-pipe inspection robots traversing through elbows,” Int. J. Robot. Theory Appl., vol. 4, no. 2, pp. 19–27, 2015.

[38] A. Kakogawa and S. Ma, “Design of a multilink-articulated wheeled pipeline inspection robot using only passive elastic joints,” Adv. Robot., vol. 32, no. 1, pp. 37–50, 2018.

[39] F. B. I. Alnaimi, A. A. Mazraeh, K. S. M. Sahari, K. Weria, and Y. Moslem, “Design of a multi-diameter in-line cleaning and fault detection pipe pigging device,” in 2015 IEEE International Symposium on Robotics and Intelligent Sensors (IRIS), 2015, pp. 258–265.

[40] C. Choi, D. Chatzigeorgiou, R. Ben-Mansour, and K. Youcef-Toumi, “Design and analysis of novel friction controlling mechanism with minimal energy for in-pipe robot applications,” in 2012 IEEE International Conference on Robotics and Automation, 2012, pp. 4118–4123.

[41] A. A. Bandala et al., “Control and Mechanical Design of a Multi-diameter Tri-Legged In-Pipe Traversing Robot,” in 2019 IEEE/SICE International Symposium on System Integration (SII), 2019, pp. 740–745.

[42] K. Tadakuma et al., “Crawler vehicle with circular cross-section unit to realize sideways motion,” in 2008 IEEE/RSJ International Conference on Intelligent Robots and Systems, 2008, pp. 2422–2428.

[43] A. V. S. Bhadoriya, V. K. Gupta, and S. Mukherjee, “Development of In-pipe Inspection Robot,” Mater. Today Proc., vol. 5, no. 9, pp. 20769–20776, 2018.

[44] A. Hadi, A. Hassani, K. Alipour, R. Askari Moghadam, and P. Pourakbarian Niaz, “Developing an adaptable pipe inspection robot using shape memory alloy actuators,” J. Intell. Mater. Syst. Struct., vol. 31, no. 4, pp. 632–647, 2020.

[45] CSIR, “Guidelines for Human Settlement Planning and Design.” CSIR Building and Construction Technology Pretoria, 2005.

[46] H. Tourajizadeh, A. Sedigh, V. Boomeri, and M. Rezaei, “Design of a new steerable in-pipe inspection robot and its robust control in presence of pipeline flow,” J. Mech. Eng. Sci., vol. 14, no. 3, pp. 6993–7016, 2020.

[47] A. H. Heidari, M. Mehrandezh, R. Paranjape, and H. Najjaran, “Dynamic analysis and human analogous control of a pipe crawling robot,” in 2009 IEEE/RSJ International Conference on Intelligent Robots and Systems, 2009, pp. 733–740.

[48] T.-J. Yeh and T.-H. Weng, “Analysis and Control of an In-Pipe Wheeled Robot With Spiral Moving Capability,” J. Auton. Veh. Syst., vol. 1, no. 1, 2021.

[49] T. Nishimura, A. Kakogawa, and S. Ma, “Pathway selection mechanism of a screw drive in-pipe robot in T-branches,” in 2012 IEEE international conference on automation science and engineering (CASE), 2012, pp. 612–617.

[50] H. Takeshima and T. Takayama, “Development of a steerable in-pipe locomotive device with six braided tubes,” ROBOMECH J., vol. 5, no. 1, pp. 1–11, 2018.

[51] A. Kakogawa and S. Ma, “An in-pipe inspection module with an omnidirectional bent-pipe self-adaptation mechanism using a joint torque control,” in 2019 IEEE/RSJ International Conference on Intelligent Robots and Systems (IROS), 2019, pp. 4347–4352.

[52] I. F. Akyildiz and E. P. Stuntebeck, “Wireless underground sensor networks: Research challenges,” Ad Hoc Networks, vol. 4, no. 6, pp. 669–686, 2006.

[53] D. R. Frankl, Electromagnetic theory. Prentice Hall, 1986.

[54] Z. Sun and I. F. Akyildiz, “Underground wireless communication using magnetic induction,” in 2009 IEEE International Conference on Communications, 2009, pp. 1–5.

[55] X. Tan, Z. Sun, and I. F. Akyildiz, “Wireless Underground Sensor Networks: MI-based communication systems for underground applications.,” IEEE Antennas Propag. Mag., vol. 57, no. 4, pp. 74–87, 2015.

[56] N. Ahmed, J. Hoyt, A. Radchenko, D. Pommerenke, and Y. R. Zheng, “A multi-coil magneto-inductive transceiver for low-cost wireless sensor networks,” in 2014 Underwater Communications and Networking (UComms), 2014, pp. 1–5.

[57] D. Wu, D. Chatzigeorgiou, K. Youcef-Toumi, and R. Ben-Mansour, “Node localization in robotic sensor networks for pipeline inspection,” IEEE Trans. Ind. Informatics, vol. 12, no. 2, pp. 809–819, 2015.

[58] R. Wu et al., “Self-powered mobile sensor for in-pipe potable water quality monitoring,” in Proceedings of the 17th International Conference on Miniaturized Systems for Chemistry and Life Sciences, 2013, pp. 14–16.

[59] D. Chatzigeorgiou, K. Youcef-Toumi, and R. Ben-Mansour, “Design of a novel in-pipe reliable leak detector,” IEEE/ASME Trans. mechatronics, vol. 20, no. 2, pp. 824–833, 2014.

[60] B. H. Lee and R. A. Deininger, “Optimal locations of monitoring stations in water distribution system,” J. Environ. Eng., vol. 118, no. 1, pp. 4–16, 1992.

[61] “SmartBall ® Inspection Report of North Beach Force Main,” 2011. Accessed: Mar. 05, 2021. [Online]. Available:

https://your.kingcounty.gov/dnrp/library/wastewater/wtd/construction/NorthBeachFM/1108_NorthBeachForceMainInspectionReport.pdf.

[62] K. Ma et al., “PipeSLAM: Simultaneous localisation and mapping in feature sparse water pipes using the Rao-Blackwellised particle filter,” in 2017 IEEE International Conference on Advanced Intelligent Mechatronics (AIM), 2017, pp. 1459–1464.

[63] R. Worley et al., “Robot Localization in Water Pipes Using Acoustic Signals and Pose Graph Optimization,” Sensors, vol. 20, no. 19, p. 5584, 2020.

[64] Y. Wu, E. Mittmann, C. Winston, and K. Youcef-Toumi, “A Practical Minimalism Approach to In-pipe Robot Localization,” in 2019 American Control Conference (ACC), 2019, pp. 3180–3187.

[65] T. Seco, C. Rizzo, J. Espelos\’\in, and J. L. Villarroel, “A robot localization system based on rf fadings using particle filters inside pipes,” in 2016 International Conference on Autonomous Robot Systems and Competitions (ICARSC), 2016, pp. 28–34.

[66] C. Rizzo, F. Lera, and J. L. Villarroel, “A methodology for localization in tunnels based on periodic RF signal fadings,” in 2014 IEEE Military Communications Conference, 2014, pp. 317–324.

[67] Y. Yan and S. Wong, “A navigation algorithm of the mobile robot in the indoor and dynamic environment based on the PF-SLAM algorithm,” Cluster Comput., vol. 22, no. 6, pp. 14207–14218, 2019.

[68] A. Ahrary, L. Tian, S. Kamata, and M. Ishikawa, “An autonomous sewer robots navigation based on stereo camera information,” in 17th IEEE International Conference on Tools with Artificial Intelligence (ICTAI’05), 2005, pp. 6--pp.

[69] T. Wu, S. Lu, and Y. Tang, “An in-pipe internal defects inspection system based on the active stereo omnidirectional vision sensor,” in 2015 12th International Conference on Fuzzy Systems and Knowledge Discovery (FSKD), 2015, pp. 2637–2641.

[70] D. Krys and H. Najjaran, “Development of visual simultaneous localization and mapping (VSLAM) for a pipe inspection robot,” in 2007 International Symposium on Computational Intelligence in Robotics and Automation, 2007, pp. 344–349.

[71] W. Zhao, L. Zhang, and J. Kim, “Design and analysis of independently adjustable large in-pipe robot for long-distance pipeline,” Appl. Sci., vol. 10, no. 10, p. 3637, 2020.

[72] W. J. Zhang and C. A. Van Luttervelt, “Toward a resilient manufacturing system,” CIRP Ann., vol. 60, no. 1, pp. 469–472, 2011.

[73] A. C. Yunus, Fluid Mechanics: Fundamentals And Applications (Si Units). Tata McGraw Hill Education Private Limited, 2010.

[74] R. Book, “Guidelines for Human Settlement Planning and Design,” Compil. under Patronage SA Dep. Hous. by CSIR Build. Constr. Technol. Div., 2004.

[75] S. Kazeminasab, A. Akbari, R. Jafari, and M. K. Banks, “Design, Characterization, and Control of a Size Adaptable In-pipe Robot for Water Distribution Systems,” 2021.

[76] “PureRobotics® - Pipeline Inspection System - Pure Technologies - Pure Technologies.” https://puretechltd.com/technology/purerobotics-pipeline-inspection-system/ (accessed Jul. 09, 2021).

[77] A. Kakogawa, T. Nishimura, and S. Ma, “Designing arm length of a screw drive in-pipe robot for climbing vertically positioned bent pipes,” Robotica, vol. 34, no. 2, pp. 306–327, 2016.

[78] V. Sankaranarayanan and A. D. Mahindrakar, “Control of a class of underactuated mechanical systems using sliding modes,” IEEE Trans. Robot., vol. 25, no. 2, pp. 459–467, 2009.

[79] J. P. Hespanha, Linear systems theory. Princeton university press, 2018.

[80] E. V. Kumar and J. Jerome, “Robust LQR controller design for stabilizing and trajectory tracking of inverted pendulum,” Procedia Eng., vol. 64, pp. 169–178, 2013.

[81] R. Mahony, T. Hamel, and J.-M. Pflimlin, “Nonlinear complementary filters on the special orthogonal group,” IEEE Trans. Automat. Contr., vol. 53, no. 5, pp. 1203–1218, 2008.

[82] H.-P. Huang, J.-L. Yan, and T.-H. Cheng, “Development and fuzzy control of a pipe inspection robot,” IEEE Trans. Ind. Electron., vol. 57, no. 3, pp. 1088–1095, 2009.

[83] L. Brown, J. Carrasco, S. Watson, and B. Lennox, “Elbow Detection in Pipes for Autonomous Navigation of Inspection Robots,” J. Intell. Robot. Syst., vol. 95, no. 2, pp. 527–541, 2019.

[84] H. M. Kim, Y. S. Choi, Y. G. Lee, and H. R. Choi, “nishimura2012,” IEEE/ASME Trans. Mechatronics, vol. 22, no. 1, pp. 227–235, 2016.

[85] L. Li, M. C. Vuran, and I. F. Akyildiz, “Characteristics of underground channel for wireless underground sensor networks,” in Proc. Med-Hoc-Net, 2007, vol. 7, pp. 13–15.

[86] R. Weinstein, “RFID: a technical overview and its application to the enterprise,” IT Prof., vol. 7, no. 3, pp. 27–33, 2005.

[87] T. Knowles, J. Larmouth, and K. G. Knightson, Standards for open systems interconnection, vol. 3. BSP Professional Books, 1987.

[88] K. Sattlegger and U. Denk, “Navigating your way through the RFID jungle,” White Pap. Texas Instruments, 2014.

[89] “SMARTRFTM-STUDIO SmartRF Studio | TI.com.” https://www.ti.com/tool/SMARTRFTM-STUDIO (accessed Nov. 18, 2020).

[90] Z. Sun and I. F. Akyildiz, “Magnetic induction communications for wireless underground sensor networks,” IEEE Trans. Antennas Propag., vol. 58, no. 7, pp. 2426–2435, 2010.

[91] “CC1200 CC1200 Low-Power, High-Performance RF Transceiver 1 Device Overview,” 2013. Accessed: Sep. 29, 2020. [Online]. Available: www.ti.com.

[92] Z. Chu, F. Zhou, Z. Zhu, R. Q. Hu, and P. Xiao, “Wireless powered sensor networks for Internet of Things: Maximum throughput and optimal power allocation,” IEEE Internet Things J., vol. 5, no. 1, pp. 310–321, 2017.

[93] H. Guo, Z. Sun, and C. Zhou, “Practical design and implementation of metamaterial-enhanced magnetic induction communication,” IEEE Access, vol. 5, pp. 17213–17229, 2017.

[94] Z. Sun, P. Wang, M. C. Vuran, M. A. Al-Rodhaan, A. M. Al-Dhelaan, and I. F. Akyildiz, “MISE-PIPE: Magnetic induction-based wireless sensor networks for underground pipeline monitoring,” Ad Hoc Networks, vol. 9, no. 3, pp. 218–227, 2011.

[95] S. Kisseleff, I. F. Akyildiz, and W. H. Gerstacker, “Throughput of the magnetic induction based wireless underground sensor networks: Key optimization techniques,” IEEE Trans. Commun., vol. 62, no. 12, pp. 4426–4439, 2014.

[96] N. R. Peplinski, F. T. Ulaby, and M. C. Dobson, “Dielectric properties of soils in the 0.3-1.3-GHz range,” IEEE Trans. Geosci. Remote Sens., vol. 33, no. 3, pp. 803–807, 1995.

[97] “Operating Manual for Micropump mp6/mp6-pp and Controller.” https://webcache.googleusercontent.com/search?q=cache:1YdHdcZAk3cJ:https://www.servoflo.com/micropumps/download/752/1074/17+&cd=1&hl=en&ct=clnk&gl=us (accessed Nov. 18, 2020).

[98] “TI.10 433MHz 0dBi Terminal Antenna SMA(M) High Temperature - Taoglas.” https://www.taoglas.com/product/ti-10-433mhz-terminal-antenna-smam-high-temperature/ (accessed Nov. 19, 2020).

[99] R. Wu, “Development of a mobile sensor for potable water quality monitoring,” Purdue University, 2014.

[100] A.-S. Feiner and A. J. McEvoy, “The nernst equation,” J. Chem. Educ., vol. 71, no. 6, p. 493, 1994.

[101] A. Kulkarni, V. Kumar, and S. B. Dhok, “Enabling technologies for range enhancement of MI based wireless non-conventional media communication,” in 2018 9th International Conference on Computing, Communication and Networking Technologies (ICCCNT), 2018, pp. 1–7.

[102] N. Ahmed, A. Radchenko, D. Pommerenke, and Y. R. Zheng, “Design and evaluation of low-cost and energy-efficient magneto-inductive sensor nodes for wireless sensor networks,” IEEE Syst. J., vol. 13, no. 2, pp. 1135–1144, 2018.

[103] Z. Sun, P. Wang, M. C. Vuran, M. A. Al-Rodhaan, A. M. Al-Dhelaan, and I. F. Akyildiz, “MISE-PIPE: Magnetic induction-based wireless sensor networks for underground pipeline monitoring,” Ad Hoc Networks, vol. 9, no. 3, pp. 218–227, May 2011, doi: 10.1016/j.adhoc.2010.10.006.

[104] A. R. Silva and M. Moghaddam, “Operating frequency selection for low-power magnetic induction-based wireless underground sensor networks,” in 2015 IEEE Sensors Applications Symposium (SAS), 2015, pp. 1–6.

[105] J. Zhou and J. Chen, “Maximum distance estimation of far-field model for underwater magnetic field communication,” in 2017 IEEE 7th Annual Computing and Communication Workshop and Conference (CCWC), 2017, pp. 1–5.

[106] D. Wu, K. Youcef-Toumi, S. Mekid, and R. Ben Mansour, “Relay node placement in wireless sensor networks for pipeline inspection,” in 2013 American Control Conference, 2013, pp. 5905–5910.

[107] D. Wu, D. Chatzigeorgiou, K. Youcef-Toumi, S. Mekid, and R. Ben-Mansour, “Channel-aware relay node placement in wireless sensor networks for pipeline inspection,” IEEE Trans. Wirel. Commun., vol. 13, no. 7, pp. 3510–3523, 2014.

[108] J. A. I. Diaz et al., “Development of an adaptive in-pipe inspection robot with rust detection and localization,” in TENCON 2018-2018 IEEE Region 10 Conference, 2018, pp. 2504–2509.

[109] A. V. Reyes-Acosta, I. Lopez-Juarez, R. Osorio-Comparán, and G. Lefranc, “3D pipe reconstruction employing video information from mobile robots,” Appl. Soft Comput., vol. 75, pp. 562–574, 2019.

[110] A. D. Tezerjani, M. Mehrandezh, and R. Paranjape, “4-DOF pose estimation of a pipe crawling robot using a Collimated Laser, a conic mirror, and a fish-eye camera,” in 2014 Southwest Symposium on Image Analysis and Interpretation, 2014, pp. 45–48.

[111] J.-S. Lee, S. Roh, H. Moon, H. R. Choi, and others, “In-pipe robot navigation based on the landmark recognition system using shadow images,” in 2009 IEEE international conference on robotics and automation, 2009, pp. 1857–1862.

[112] H. Qi, X. Zhang, H. Chen, and J. Ye, “Tracing and localization system for pipeline robot,” Mechatronics, vol. 19, no. 1, pp. 76–84, 2009.

[113] H. Qi, J. Ye, X. Zhang, and H. Chen, “Wireless tracking and locating system for in-pipe robot,” Sensors Actuators A Phys., vol. 159, no. 1, pp. 117–125, 2010.

[114] S. Kazeminasab, R. Jafari, and M. K. Banks, “An LQR-assisted Control Algorithm for an Under-actuated In-pipe Robot in Water Distribution Systems,” 2021.

[115] W. He, Z. Li, and C. L. P. Chen, “A survey of human-centered intelligent robots: issues and challenges,” IEEE/CAA J. Autom. Sin., vol. 4, no. 4, pp. 602–609, 2017.

[116] X. Yu, W. He, H. Li, and J. Sun, “Adaptive fuzzy full-state and output-feedback control for uncertain robots with output constraint,” IEEE Trans. Syst. Man, Cybern. Syst., 2020.

[117] A. Ahrary, Y. Kawamura, and M. Ishikawa, “A laser scanner for landmark detection with the sewer inspection robot KANTARO,” in 2006 IEEE/SMC International Conference on System of Systems Engineering, 2006, pp. 6--pp.

[118] D. Alejo, F. Caballero, and L. Merino, “A robust localization system for inspection robots in sewer networks,” Sensors, vol. 19, no. 22, p. 4946, 2019.

[119] R. Worley, Y. Yu, and S. Anderson, “Acoustic Echo-Localization for Pipe Inspection Robots,” in 2020 IEEE International Conference on Multisensor Fusion and Integration for Intelligent Systems (MFI), 2020, pp. 160–165.

[120] K.-U. Scholl, V. Kepplin, K. Berns, and R. Dillmann, “Controlling a multi-joint robot for autonomous sewer inspection,” in Proceedings 2000 ICRA. Millennium Conference. IEEE International Conference on Robotics and Automation. Symposia Proceedings (Cat. No. 00CH37065), 2000, vol. 2, pp. 1701–1706.

[121] N. M. H. Basri, K. S. M. Sahari, and A. Anuar, “Development of a robotic boiler header inspection device with redundant localization system,” J. Adv. Comput. Intell. Intell. Informatics, vol. 18, no. 3, pp. 451–458, 2014.

[122] C. hyeuk Lee, D. Joo, G. ho Kim, B. soo Kim, G. hoon Lee, and S. geul Lee, “Elbow detection for localization of a mobile robot inside pipeline using laser pointers,” in 2013 10th International Conference on Ubiquitous Robots and Ambient Intelligence (URAI), 2013, pp. 71–75.

[123] D. Zhao and W. Whittaker, “High Precision In-Pipe Robot Localization with Reciprocal Sensor Fusion,” arXiv Prepr. arXiv2002.12408, 2020.

APPENDIX

Journal Papers

1. Saber Kazeminasab, Roozbeh Jafari, and M. Katherine Banks “SmartCrawler: An In-pipe Size-adaptable Robotic System with Multi-phase Motion Control Algorithm and Wireless Sensor Module for Water Quality Monitoring in Water Distribution Systems”, Robotics and Autonomous Systems [Submitted, Under Review]
2. Saber Kazeminasab, Roozbeh Jafari, and M. Katherine Banks “A Localization and Navigation Method for an In-pipe Robot in Water Distribution System through Wireless Control” [In Preparation].
3. Saber Kazeminasab, Roozbeh Jafari, and M. Katherine Banks “Towards Long Distance Inspection for In-pipe Robot in Water Distribution Systems” [In Preparation].

Conference Papers

1. Saber Kazeminasab, Roozbeh Jafari, and M. Katherine Banks, “An LQR-assisted Control Algorithm for an Under-actuated In-pipe Robot in Water Distribution Systems” The 36th ACM/SIGAPP Symposium On Applied Computing, Virtual Conference, March 2021
2. Saber Kazeminasab, A. Akbari, Roozbeh Jafari, and M. Katherine Banks, “Design, Characterization, and Control of a Size Adaptable In-pipe Robot for Water Distribution Systems” 22nd IEEE International Conference on Industrial Technology (ICIT), Virtual Conference, 2021.
3. Saber Kazeminasab, Roozbeh Jafari, M. Katherine Banks, “Design and Control of a Self-rescue Mechanism for an Under-actuated In-pipe Robot for Obstacle-avoidance in Water Distribution Systems”.